



Extracellular Vesicles in Human Plasma

Improving Diagnostics of *EGFR* T790M Mutation Detection in NSCLC

Hilven Winde

Supervisor
Van Hoof Rebekka

Promotor
Nelissen Inge

Internship mentor
Sabine Van Miert

Bachelor's in Biomedical Laboratory Technologies

Option: Pharmaceutical and Biological Laboratory
Technologies

Academic year: 2021-2022

Campus Geel, Kleinhoefstraat 4, BE-2440 Geel

LID VAN

**ASSOCIATIE
KU LEUVEN**

THOMAS
MORE

PREFACE

This research was performed for my internship at VITO (Vlaams Instituut voor Technologisch Onderzoek), which is an essential element of a bachelor's degree in biomedical laboratory technology.

During this internship I learned a variety of new techniques, I learned to work with cancer-cell lines and how to collect extracellular vesicles from cells and plasma samples. The different analysis methods learned are bio layer interferometry, digital droplet PCR, nano particle tracking analysis, western blot.

I'm very thankful for all the opportunities, as well as the possibilities for personal growth I have experienced at VITO.

I would like to thank my supervisor Rebekka Van Hoof, for helping me with all the practical work, helping me understanding the science behind things and for reviewing my thesis so often.

I am also very thankful for my internship mentor Sabine van Miert, for giving thorough feedback on my thesis and making time for face to face feedback sessions.

Another person who deserves credits for the outcome of this thesis is Inge Nelissen. Thank you for giving feedback on my thesis and helping with processing of my results in our meetings.

Some other people that deserve to be put in the spotlight: An Jacobs for explaining how to implement the nano particle tracking analysis; Carmen Ter Heide for helping me in the lab and at our desks; Karen Hollander for explaining all the safety measures in the lab; Pascale Berckmans for measuring and processing the flow cytometry data.

And of course, thank you to all the people at VITO for always helping me when needed.

Last but not least I would also like to thank my family for proofreading this thesis and supporting me when needed.

SUMMARY

Lung cancer mutation detection in patients currently happens by taking tissue biopsies. This method is invasive and does not guarantee a representative diagnosis for the whole tumor. A non-invasive alternative is liquid biopsies, with this method cell-free tumor DNA and circulating tumor cells can be analyzed in biological fluids like blood. However, they are mostly present in later stages of the disease. Therefore, there has been a great interest in markers that are available at early cancer stages such as extracellular vesicles (EVs). These vesicles are released in the bloodstream for communication and they contain the same mutations as the cancer cells they originated from. In this thesis, methods were optimized to improve mutation detection of the point mutation T790M in the epidermal growth factor receptor (*EGFR*) gene in extracellular vesicles derived from the human NCI-H1975 lung cancer cell line.

The influence of two different blood collection tubes on blood-derived EV concentration, total protein amount and presence of EV-related protein markers was evaluated. The used RNA Complete blood collection tubes were best suited for EV stabilization, while the cell-free DNA tubes contained a higher total protein concentration. Additionally, bio-layer Interferometry was optimized for EV-binding using NCI-H1975 cell line-derived EVs containing the *EGFR* T790M mutation. A clear negative signal was produced by EV-binding. Conformation of EV binding was proven in a gold nanoparticle sandwich assay. There was a linear correlation between the used EV concentration and the measured signal after 3000 seconds. A larger binding signal was observed when using the anti-EV-associated protein CD81 antibody compared to the binding signal of EVs when using the anti-CD9 antibody. Digital PCR was used to investigate the presence of *EGFR* T790M in the captured EVs. There was no clear correlation observed between mutation quantity and EVs used for binding. This can be explained by the presence of free DNA fragments.

This project provided insights into the suitability of EVs for cancer mutation detection, and tools to improve future EV-based molecular diagnostics. Evaluation of a larger number of blood samples and variations between different plasma samples is still required for more concrete conclusions.

SAMENVATTING

Het opsporen van mutaties in longkanker bij patiënten gebeurt momenteel door het nemen van weefselbiopsieën. Deze methode is invasief en garandeert niet dat er een representatieve diagnose voor de gehele tumor wordt waargenomen. Een niet-invasief alternatief zijn vloeibare biopsieën, waarbij cel vrij tumor-DNA en circulerende tumorcellen kunnen worden geanalyseerd in biologische vloeistoffen zoals het bloed. Deze zijn echter meestal aanwezig in latere stadia van de ziekte. Daarom is er grote belangstelling voor merkers die in een vroeg stadium van kanker beschikbaar zijn, zoals extracellulaire vesicles (EVs). Deze vesicles komen vrij in de bloedbaan voor cel communicatie en bevatten dezelfde mutaties als de kankercellen waarvan ze afkomstig zijn. In dit eindwerk werden methoden geoptimaliseerd om de mutatiedetectie te verbeteren van de puntmutatie T790M in het epidermale groeifactor receptor (*EGFR*) gen in extracellulaire vesicles afkomstig van de menselijke NCI-H1975 longkankerlijn.

De invloed van twee verschillende bloedafnamebuisjes op de EV-concentratie in het bloed, de totale hoeveelheid proteïnen en de aanwezigheid van EV-gerelateerde proteïnermarkers werd geëvalueerd. De gebruikte RNA Complete bloedafnamebuisjes waren het best geschikt voor EV-stabilisatie, terwijl de cell-free DNA-bloedafnamebuisjes een hogere totale proteïne concentratie aantoonde. Bovendien werd bio-laaginterferometrie geoptimaliseerd voor EV-binding met NCI-H1975 cellijn afgeleide EVs die de *EGFR* T790M mutatie bevatten. Er werd een duidelijk negatief signaal geproduceerd door EV-binding. Conformatie van EV-binding werd aangetoond met behulp van een gouden nanodeeltjes sandwich assay. Er was een lineaire correlatie tussen de gebruikte EV-concentratie en het gemeten signaal na 3000 seconden. Een groter bindingssignaal werd waargenomen bij gebruik van het anti-EV-geassocieerd proteïne CD81 antilichaam in vergelijking met het bindingssignaal van EVs bij gebruik van het anti-CD9 antilichaam. Digitale PCR werd gebruikt om de aanwezigheid van *EGFR* T790M in de gevangen EVs te onderzoeken. Er werd geen duidelijke correlatie waargenomen tussen de hoeveelheid mutaties en de EVs die gebruikt werden voor binding. Dit kan verklaard worden door de aanwezigheid van vrije DNA-fragmenten.

Dit project gaf inzicht in de bruikbaarheid van EVs voor het opsporen van kankermutaties en mogelijkheden om toekomstige EV-gebaseerde moleculaire diagnostiek te verbeteren. Verdere evaluatie van een groter aantal bloedstalen en variaties tussen verschillende plasma monsters is nodig voor meer concrete conclusies.

TABLE OF CONTENTS

PREFACE.....	2
SUMMARY	3
SAMENVATTING	4
TABLE OF CONTENTS	5
ABBREVIATIONS	7
INTRODUCTION	8
1 LUNG CANCER	10
2 EXTRACELLULAR VESICLES	12
2.1 Function and applications of EVs	13
2.2 EV isolation from plasma.....	13
3 ANALYSIS PRINCIPLES	15
3.1 Bio-layer Interferometry	15
3.2 Droplet Digital PCR.....	16
4 MATERIALS AND METHOD	18
4.1 Blood collection and plasma preparation	18
4.2 Plasma EV separation	19
4.2.1 qEV.....	19
4.2.2 Smart size exclusion chromatography	19
4.3 Cell culture and EVs.....	20
4.3.1 Cell cultivation	20
4.3.2 Cell EV production	20
4.4 NCI-H1975 EV preparation	20
4.4.1 SEC and ultracentrifugation.....	21
4.4.2 Ultracentrifugation	21
4.5 EV characterization	21
4.5.1 Western blot	21
4.5.2 Nanoparticle tracking analysis	23
4.5.3 Protein concentration determination	23
4.5.4 High-sensitivity flow cytometry.....	24
4.5.5 Bio-layer Interferometry	26
4.5.6 ddPCR.....	27
5 RESULTS.....	29
5.1 Effect of blood collection tubes on the EV fraction.....	29
5.1.1 Protein analysis	29
5.1.2 High-sensitivity flow cytometry.....	33
5.2 Evaluation of DNA mutation detection in specific EV subpopulations captured by BLI	35
5.2.1 Characterization of NCI-H1975 cell line-derived EVs	35
5.2.2 Optimization of EV binding	36

5.2.3 Sandwich assay with anti-CD9 antibody conjugated gold nanoparticles .38
5.2.4 Downstream analysis of captured EV content38
6 DISCUSSION41
CONCLUSION.....43
REFERENCE LIST.....44
ATTACHMENTS47

ABBREVIATIONS

BCT	blood collection tube
BLI	bio-layer interferometry
CFDA	carboxyfluorescein diacetate succinimidyl ester
CMG	CellMask™ Green
ctDNA	circulating tumor deoxynucleic acid
ddPCR	droplet digital polymerase chain reaction
DNA	deoxyribonucleic acid
EGFR	epidermal growth factor receptor
EV(s)	extracellular vesicle(s)
FBS	fetal bovine serum
KRAS	Kirsten rat sarcoma viral oncogene homolog
mRNA	messenger ribonucleic acid
NSCLC	non-small-cell lung carcinoma
NTA	nano particle tracking analysis
PBS	phosphate buffered saline
PFP	platelet-free plasma
RNA	ribonucleic acid
SA	streptavidin
SEC	size exclusion chromatography
SP-SSC	small particle side scatter
TKI	tyrosine kinase inhibitor

INTRODUCTION

Almost everyone has come into (direct) contact with the devastating effects of cancer. In Belgium, cancer is the cause of 25% of the total number of deaths (Belgische Federale Overheidsdiensten, 2021). The cancer that causes the most deaths worldwide is lung cancer (Bray et al., 2018). Lung cancer is hard to find in its early stages because of its asymptomatic nature, this leads to low-efficiency treatments and a higher chances of death (Wang et al., 2018). Diagnostic methods currently used are X-rays, sputum collection, bronchoscopies, and biopsies. These conventional screening methods are inefficient in detecting early lung cancer, and sputum collection, as well as bronchoscopies give the patient a high discomfort level (Yuan et al., 2021).

The most prevalent form of lung cancer is non-small-cell lung carcinoma (NSCLC). This type of cancer is treated with tyrosine kinase inhibitors (TKIs) which are less toxic than upfront chemotherapy. A very common problem is that the patient's cancer cells acquire a mutation in the epidermal growth factor receptor (EGFR) which makes the carcinoma resistant to this type of treatment (Zhang et al., 2010). This mutation is not easily noticed. Currently, the only way of getting a thorough follow-up of the mutation state is by taking a tissue biopsy. This can show a deviating view on the overall picture because a mutated cell can be missed if it's not located at the biopsy site. The indicated sample collection is also very invasive (Travis et al., 2013).

Blood sample collection can be of great help in minimally invasive monitoring of the cancer mutation status in a patient. Blood collection is easy, quick, and can happen routinely at the doctor's office. These liquid biopsies are already used to detect circulating tumor DNA (ctDNA) or circulating tumor cells. A major problem with these methods is that the sensitivity for these kind of biomarkers is too low in early cancer stages (Punnoose et al., 2012; Wan et al., 2018). Recent investigations suggest that extracellular vesicles (EVs) could provide a solution for this low sensitivity (Hur et al., 2018). Extracellular vesicles are excreted by all cells, including malignant cells, and enter the bloodstream (Neven et al., 2017). Inside and at the outer membrane of the EVs, different molecules of the original cell are transported (Neven et al., 2017). Some of these molecules are DNA and RNA which contain the same mutations as the lung carcinoma cells. This EV-associated DNA is protected by the bilipid membrane of the vesicle and suffers less from degradation compared to ctDNA, therefore it can be a more stable source for mutation detection and genetic analysis (Wan et al., 2018).

By specifically capturing the EVs derived from cancer cells and subsequently analyzing the cargo of these particles, it is possible to deliver personal and specific treatment based on the mutation profile of a patient. A treatment that is specialized for a specific mutation or a set of mutations can fight the disease more efficiently (Lai et al., 2014). Because blood collection is less invasive than taking a tissue biopsy, it can widely be applied for screening people with a higher risk and help to detect cancer at an earlier stage. In addition, when a certain treatment is applied it allows for follow-up and quick adjustment of the therapy when necessary. This will improve the prognosis for lung cancer patients (AlQahtani et al., 2021).

In this work, we aimed to optimize methods and technologies for early mutation detection using EVs. In the first part, different factors influencing EV isolation and

DNA extraction were investigated using plasma samples from healthy human volunteers. The type of blood collection tube and its stabilizing components can influence the EV amount in the collected sample. Two different collection tubes and their impact on EVs stabilization were analyzed. Another interesting factor is the purification method that is used to remove the most unwanted interfering molecules. Two different size exclusion chromatography (SEC) methods were compared by evaluating the isolated EVs amount and protein contents. The second part was the development of an application of EV binding and subsequent mutation detection. On a commercial bilayer platform. Cell line-derived EVs from NSCLC cells with a known EGFR mutation were used for optimization of EV capture and genetic analysis of the vesicle-content.

1 Lung cancer

There are two subtypes of lung cancer: small cell lung carcinoma and non-small-cell lung carcinoma (NSCLC). The most frequent type of lung cancer is NSCLC with 85% of all lung cancer cases (AIQahtani et al., 2021). NSCLC can be further divided into “squamous cell carcinoma”, “adenocarcinoma” and “not otherwise specified” subtypes. Characterization of the kind of cancer is important for determining the most optimal treatment. The characterization of lung cancer is sometimes done by taking a biopsy of the tumor cells. This is an invasive surgery for the patient and can give a false diagnosis of the cancer characteristics. Deviating diagnosis can be caused by heterogeneity within the tumor (Travis et al., 2013).

When patients undergo treatments, it is possible that a secondary mutation in the cancer cells arises. These kinds of mutations make the cancer cells resistant to the applied therapy and give the patient a lower chance of effective treatment. The detection of cancer mutations is becoming an important predictive biomarker for drug response. Two of the most important genes that can mutate and have a considerable role in cancer are those encoding epidermal growth factor receptor (*EGFR*) and Kirsten rat sarcoma viral oncogene homolog (*KRAS*) which influence cell proliferation, enhanced cell motility, apoptosis, and neoangiogenesis (Das et al., 2015).

The most common recurrent gene abnormality in NSCLC is an *EGFR* mutation according to Das et al. (2015). Over the last 40 years, elevated EGFR levels have been identified as a frequent component of numerous cancer types (Nicholson et al., 2001). Therefore, the EGFR T790M mutation is the focus point of this thesis.

The EGFR is a transmembrane receptor with a tyrosine kinase activity. This receptor is composed of three regions, a cytoplasmic region, an extracellular ligand-binding region, and a transmembrane helix region. The tyrosine kinase domain takes up 50% of the cytoplasmic region (Figure 1) (Zhang et al., 2010). This receptor is responsible for facilitating many intracellular signaling pathways (AIQahtani et al., 2021). Different mutations in *EGFR* influence the response to tyrosine kinase inhibitors (TKIs) as therapy, TKI therapy can supersede chemotherapy with higher specificity for the EGFR on lung cancer cells (Lu et al., 2018).

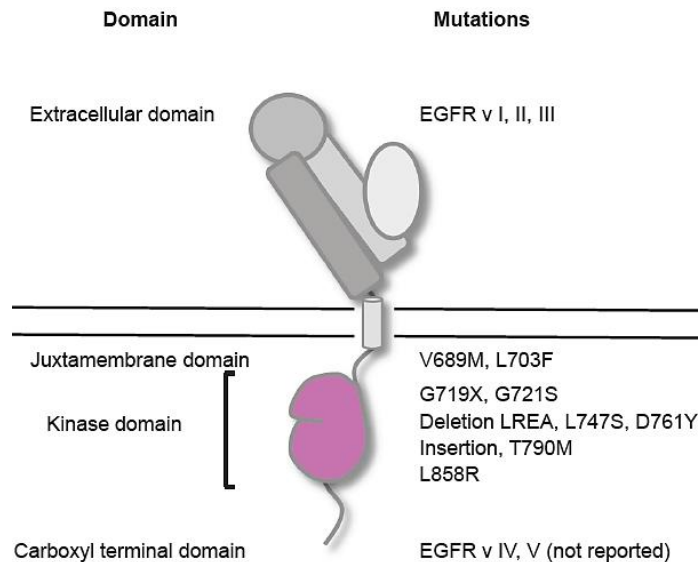


Figure 1. Positions of key *EGFR* mutations/variants in the corresponding protein domains: Extracellular and internal domain mutations of the receptor

Note. acquired from Zhang, Z., et al. (2010). *EGFR*-mutated lung cancer: a paradigm of molecular oncology. *Oncotarget*, Vol. 1 (No 7), DOI:10.18632/oncotarget.186.

The binding of the epidermal growth factor to its receptor causes autophosphorylation. This activates pathways that stimulate cell proliferation, metastasis, migration, and prevent apoptosis. Activating mutations on *EGFR* within the Caucasian population are found in 10% - 15% of NSCLC (Ricordel et al., 2018). By administering TKIs intrinsic apoptosis pathways in *EGFR*-mutant cancer cells are successfully induced (Lai et al., 2014).

A big problem with this therapy is the acquisition of a secondary resistance mutation in the *EGFR* gene which is called the T790M amino acid substitution. The T790M mutation is present in 50% to 60% of acquired resistances to *EGFR* TKIs, leading to treatment failure (Song et al., 2016). T790M is caused by a point mutation in the *EGFR* gene which leads to a substitution of threonine to methionine at amino acid position 790 in the protein. This induces steric hindrance that prevents inhibitors from binding on the receptor (Walter et al., 2013). The *EGFR* T790M mutation is treated with specialized medication and thus, detecting this mutation in NSCLC patients is of critical importance (Lu et al., 2018). In this thesis, a human NSCLC cell line NCI-H1975, carrying this *EGFR* T790M mutation was used.

2 Extracellular vesicles

Extracellular vesicles (EVs) are a heterogeneous group of nano-sized particles with a lipid bilayer membrane. These particles cannot replicate by themselves, are naturally released by cells, and do not contain a nucleus (They et al., 2018). EVs can work as a communication tool, they shuttle functional nucleic acids and proteins between the cells. A criterium that these particles must meet to be classified as EVs, is that they are present in extracellular fluids. These fluids can be cell culture medium or body fluids like blood and urine (Lotvall et al., 2014).

Initially, these particles were believed to be cell artifacts that contain unwanted material from cells, with no interesting properties (Abels & Breakefield, 2016). Further research showed an intricate mechanism of cell-to-cell communication. Because of the knowledge that cells secrete these EVs on a normal basis, opportunities for using EVs in biotechnology emerged, this will be further explained under 2.1 (Neven et al., 2017). Different types of EVs are known, these vary in size and origin. The most common subclasses are exosomes, microvesicles, apoptotic bodies, and oncosomes (Figure 2).

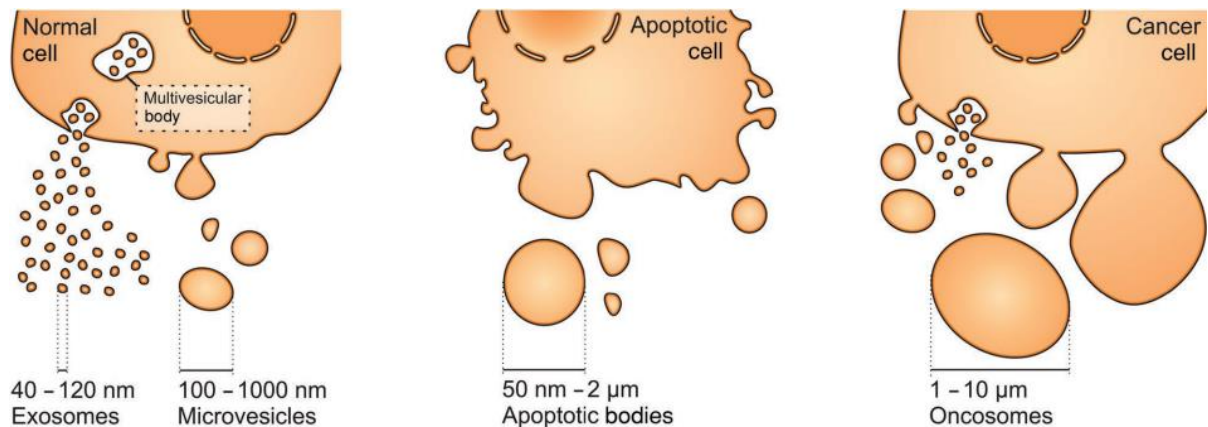


Figure 2. Extracellular vesicle and their expected size range: exosomes, microvesicles, apoptotic bodies, and oncosomes

Note. acquired from Zaborowski, M., et al. (2015). *Extracellular Vesicles: Composition, Biological Relevance, and Methods of Study*. *BioScience*, Vol. 65 (issue 8), DOI: [10.1093/biosci/biv084](https://doi.org/10.1093/biosci/biv084)

Exosomes (40–120 nm) and microvesicles (100–1000 nm) are secreted by cells in the human body and are the smallest bilayer particles. The cellular exosomes are made through intraluminal budding of the endosomal membrane during the maturation of multivesicular endosome. Fusion of this multivesicular body with the plasma membrane is visible in Figure 2. Microvesicles are generated by outward budding of the cell membrane. Apoptotic bodies (50–2000 nm) are created when a cell undergoes apoptosis. These can differ in content between biofluids. Cancer cells produce the largest vesicles, oncosomes (1–10 µm), mostly in later stages of cancer evolution (El Andaloussi et al., 2013; van Niel et al., 2018; Zaborowski et al., 2015). Apoptotic bodies and oncosomes are not desired as a target for this project.

Given the fact that we use isolation methods based on EV size in this project, we cannot discriminate between exosomes and microvesicles, and refer to the isolated vesicles as EVs.

When exosomes or microvesicles are formed, they incorporate cell plasma membrane proteins from their original cell in their lipid duplex layer (Doyle & Wang, 2019). These transmembrane proteins can be used to characterize which cell type the EVs originated from. Some general transmembrane proteins EVs can carry are CD9 and CD81 (Attachment 1) which will be used in this project for EV capture optimization. The nucleic acid inside EVs represents the DNA and RNA from its origin cell (Schubert & Boutros, 2021). These nucleic acids mirror the tumor mutation status, according to Schubert and Boutros (2021) and Thakur et al. (2014). Detecting tumor mutations with EVs is the goal of this research.

2.1 Function and applications of EVs

Recently, research (El Andaloussi et al., 2013; Yanez-Mo et al., 2015) has shown that EVs are important mediators of intercellular communication. The vesicles have an impact on fundamental biological processes in different ways. They can bind on receptors of cells, directly activating cell surface receptors via ligands, or merge with the cell membrane and deliver their contents into the recipient cell, thus delivering effectors. These effectors can be transcription factors, oncogenes, small and large non-coding regulatory RNAs, mRNAs, and infectious particles.

Currently, strong evidence suggests that EV production is omnipresent across all kingdoms of life, and that both eukaryotic and prokaryotic microbes use EVs to transport RNA (Tsatsaronis et al., 2018).

A new emerging application for EVs is using EVs as vectors for delivering drug compounds or modulating cell functions in an *in vivo* context. This is possible because EVs are biocompatible with the target cells, can be immunologically inert and if necessary be patient-derived which makes them less likely to trigger immune responses (van Niel et al., 2018).

However, this thesis is focused on the biomarker properties of EVs, and the possibilities for cancer diagnosis in liquid biopsies. Chin and Wang (2016) note that cancer cells secrete more and different EVs than normal cells. This because cancer cells undergo different cellular stresses which induce EV formation and content variation. This is a positive characteristic for biomarker diagnosis possibilities.

2.2 EV isolation from plasma

Extracellular vesicles can be found in biological fluids such as plasma, urine, blood, serum, saliva, nasal and bronchial fluid, breast milk, amniotic fluid, and seminal fluid (Yanez-Mo et al., 2015). Plasma is a component of the blood that can be retrieved by centrifugation to remove blood cells and platelets. This fraction is used in this research instead of whole blood because it contains EVs of both blood and tissue cells, including our target cancer cells. This fraction also contains significantly lower amounts of platelet EVs than serum (Palviainen et al., 2020).

By isolating the EVs contained in plasma, the content of specific EVs can be investigated. This can be a difficult task, since plasma contains different biomolecules that have some characteristics in common with EVs (Figure 3). Separation of EVs

based on their size or density can lead to co-purification of other particles such as lipoproteins, proteins, etc. that have a common size or density, respectively. A combination of multiple isolation techniques can be required to obtain a pure EV fraction (Tian et al., 2020).

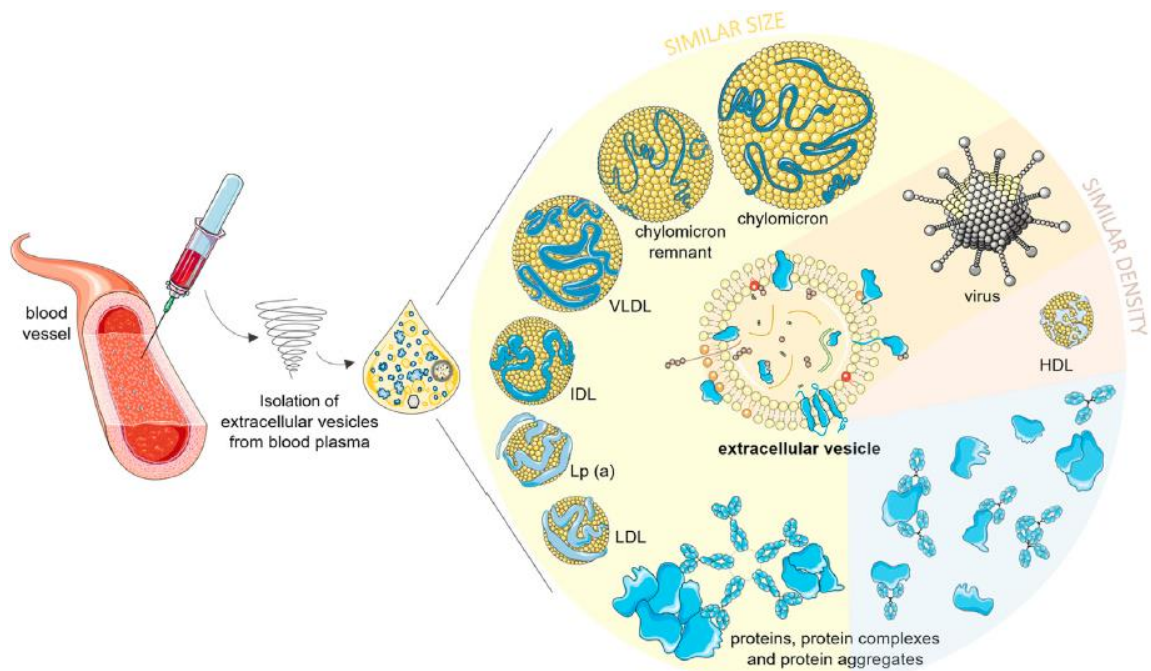


Figure 3. Overview of different particles in plasma that can cause contamination in EV samples: Lipoproteins larger than high-density lipoproteins (HDL), Protein aggregates/complexes, and viruses can have a similar size or density to the EVs in a plasma sample. (LDL, low-density lipoprotein; Lp, lipoprotein; IDL, intermediate-density lipoprotein; VLDL, very-low-density lipoprotein; EV, extracellular vesicle)

Note. acquired from Holcar, M., et al. (2021). Blood Nanoparticles – Influence on Extracellular Vesicle Isolation and Characterization. *Frontiers in Pharmacology*, Vol. 12, <https://doi.org/10.3389/fphar.2021.773844>

Components that are in plasma on a normal basis can cause interference, but another problem that influences mutation detection and collection of EVs is the variability in the amount of EVs. This quantity can vary by the influence of different factors, such as hypoxia, autophagy, and stress. Increased release and high concentrations of EVs in plasma have been reported in connection with several cancers (Holcar et al., 2021). Other factors can also influence the EVs present in a blood plasma sample like age, diet, lifestyle, etc. of the donor. But these factors cannot easily be altered.

In addition, the method of plasma preparation can also influence the EV amount in the collected sample. In this thesis the impact of the blood collection tube, the time between collection and plasma preparation, the preparation method, and the preservation method is observed. In contrast, sample tube manipulation and transportation can be easily optimized and standardized.

3 Analysis principles

3.1 Bio-layer Interferometry

Bio-layer interferometry (BLI) is an optical technique that analyses interference patterns between waves of light to measure macromolecular interactions (Figure 4). This technique uses white light directed down a biosensor tip towards two interfaces that are separated by a thin layer. The tip has an external surface that can be conjugated with an affinity molecule (e.g. antibody or aptamer) and an internal reference layer. The interference patterns that are formed between these layers are analyzed with a detector. When target molecules bind to the exposed biolayer of affinity molecules, the shift of interference patterns can be measured in real-time (Center for Macromolecular Interactions, 2022) (Jacobs, 2021).

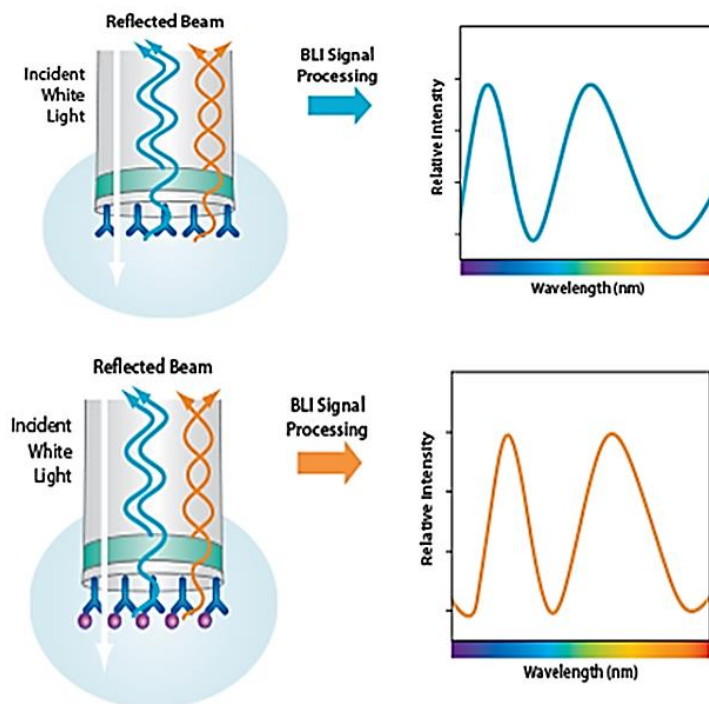


Figure 4. Bio-layer Interferometry (BLI) principle. The molecular binding causes a shift in wavelength of the BLI signal

Note. acquired from Sartorius AG (2022). Bio-layer Interferometry (BLI) Label-Free Technology. Sartorius [Website]. Consulted on 15 February 2022 via [BLI Technology | Sartorius](#)

The technique is performed in an open top shaking micro well plate, using disposable interchangeable optical fiber biosensor tips. The principle of this technique is based on the correlation of the spectral shift in wavelength with a change in the number of particles bound on the biosensor surface. This platform allows measurement of kinetics and affinity of biomolecular interactions (Wallner et al., 2019).

In this project, a BLI application was developed for reproducible binding and quantification of a specific sub-population of EVs, derived from NCI-H1975. For this a specific antibody-based assay was optimized that recognizes two specific EV membrane proteins, CD9 and CD81. The time kinetic profile of specifically binding EVs is observed to determine optimal antibody binding. This application has the potential to increase the sensitivity of mutation detection in specific cancers.

3.2 Droplet Digital PCR

Droplet digital polymerase chain reaction (ddPCR) minimizes sample dilution and increases the precision and quantification options for DNA and RNA analyses. ddPCR can measure absolute quantities by counting nucleic acid molecules with the help of fluorescent probes. These molecules are encapsulated in volumetrically defined water-in-oil droplet partitions (Bio-Rad, 2022). The principle of the ddPCR can be seen in Figure 5.

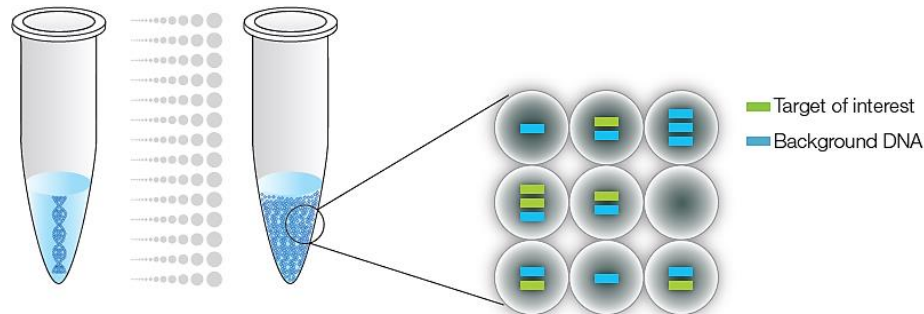


Figure 5. Droplet digital PCR principle. DNA strands are separated into droplets and can now be visualized as individual strands, instead of being a small amount in a large pool of different DNA

Note. Acquired from Bio Rad (2022). Droplet Digital PCR Applications Guide [manual]. Bio-Rad. Consulted on 16 February 2022 via [Bulletin_6407.pdf \(bio-rad.com\)](#)

The sample volume is partitioned into oil-based droplets that each contain small amounts of DNA. This conversion makes it easier to find one mutation in a target gene in comparison to one large sample volume with both mutant and wild-type DNA. Target and background DNA are randomly distributed into the droplets (Tong et al., 2017). Because of this partition, there is a precise target amplification and quantification. By adding fluorescent labels to the DNA, positive droplets which contain at least one copy of target DNA show increased fluorescence compared to negative droplets. The measuring device detects the fluorescence emitted by the droplets and calculates the chance of multiple molecules being in one droplet based on the amount of measured empty droplets. Thus, absolute quantification of the target is possible (Bio-Rad, 2022).

Fluorescence is produced by the used probes. When the probe is intact the fluorescence of the reporter is quenched due to proximity to the quencher. The probe binds to a specific target sequence during annealing. While the DNA gets extended the probe is cleaved from the target, this frees the reporter (FAM/HEX) from the quencher and produces a fluorescent signal proportional to amplified amounts of target in the sample (Figure 6) (Bio-Rad, 2022).

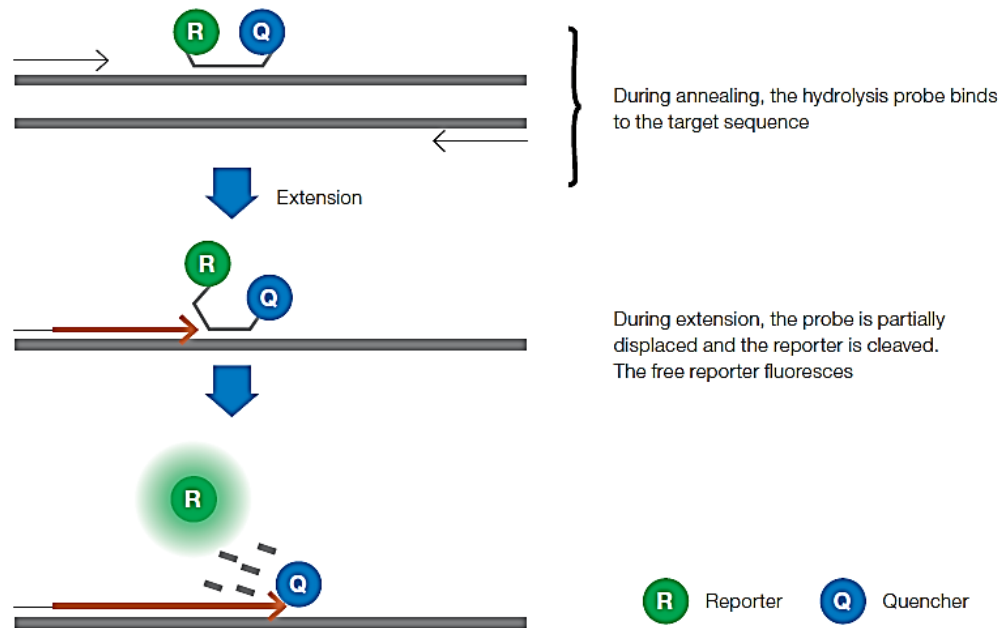


Figure 6. Fluorescent probe operation process: the probe binds a target sequence on the DNA strand, during elongation this probe is cut, and the fluorescent signal is emitted

Note. Acquired from Bio Rad (2022). *Droplet Digital PCR Applications Guide [manual]*. Bio-Rad. Consulted on 27 March 2022 via [Bulletin_6407.pdf \(bio-rad.com\)](#)

This measurement principle will be used to detect the quantity of *EGFR* T790M mutation present on BLI tips after EV capture. With a FAM or HEX dye label on the TaqMan probes the wild-type and mutated genes can be discriminated in a sample.

4 Materials and Method

4.1 Blood collection and plasma preparation

The plasma samples used for the EV separation were collected by venipuncture on 16 March and 27 April 2022 at the medical department of SCK CEN. Ethical approval for this study was obtained from the Central Ethical Committee of the University Hospital Antwerp. Healthy volunteers of the SCK CEN/VITO personnel donated two or four 10 mL blood collection tubes (BCTs) after signing the informed consent. The used blood collection tubes are displayed in Figure 7. These tubes are designed to stabilize cell-free DNA (left tube) or cell-free RNA and EVs (right tube) in the sample after blood collection, respectively, and were compared for the EV stability. We investigated the difference in EV stability after immediate (<2h) or after five days of storage at room temperature before processing the blood to plasma.



Figure 7. Cell-free DNA (left) and RNA Complete (right) blood collection tube from Streck.

Note. Acquired from System Streck© (2022). Stabilization. Streck© [Website]. Consulted on 7 April 2022 via [Cell-Free DNA BCT RUO & CE - Streck](#) and [RNA Complete BCT for Cell-Free RNA \(cfRNA\)-Streck](#)

The collected blood samples were processed to plasma following the protocol described by Lacroix et al. (2013) to remove thrombocytes.

The BCTs were centrifugated for 15 minutes at 2500 g (or 5095 RPM) using the EBA 20, Hettich centrifuge at room temperature. The plasma was aspirated up to one centimeter above the buffy coat and transferred to a 15mL collection tube made from polypropylene (Corning). The collected plasma was centrifuged again at the same settings. Next, the plasma was aspirated and placed in a fresh 15 mL tube leaving 100 μ L at the bottom of the previous tube. The resulting platelet-free plasma (PFP) was divided in protein LoBind® Eppendorf tubes in fractions of 1.2 mL and stored at -80 °C until further use.

Plasma that was separated after five days of storage at room temperature, was separated on 2 May 2022.

4.2 Plasma EV separation

Two commercially available size exclusion chromatography-based (SEC) EV separation kits were compared to evaluate the impact on the protein contents and EV concentration in the collected plasma samples. For each method, 500 μ L of PFP was processed to obtain purified PFP EV fractions.

4.2.1 qEV

A qEVoriginal 70 nm column (Izon Science Ltd.) was used according to the manufacturer's protocol (IZON sciences, 2022). The column was rinsed with 15 mL 0.1 μ m filtered PBS before each use and used for five purifications per column. When the column was stored and not fully used 20% ethanol was run through for disinfection and flushing of the column. The column was then stored at 4 $^{\circ}$ C.

To collect the EV fractions of the samples, 500 μ L of PFP sample was placed on the column, and 13 fractions of 0.5 mL were collected. The fractions were collected in protein LoBind[®] Eppendorf tubes, aliquoted and stored at -80 $^{\circ}$ C until further use.

4.2.2 Smart size exclusion chromatography

The SmartSEC[®] HT EV Isolation System for Serum & Plasma (System Biosciences) was used according to the manufacturer's protocol (Smart SEC System, 2022). The plasma clearing step is shown in Figure 8.

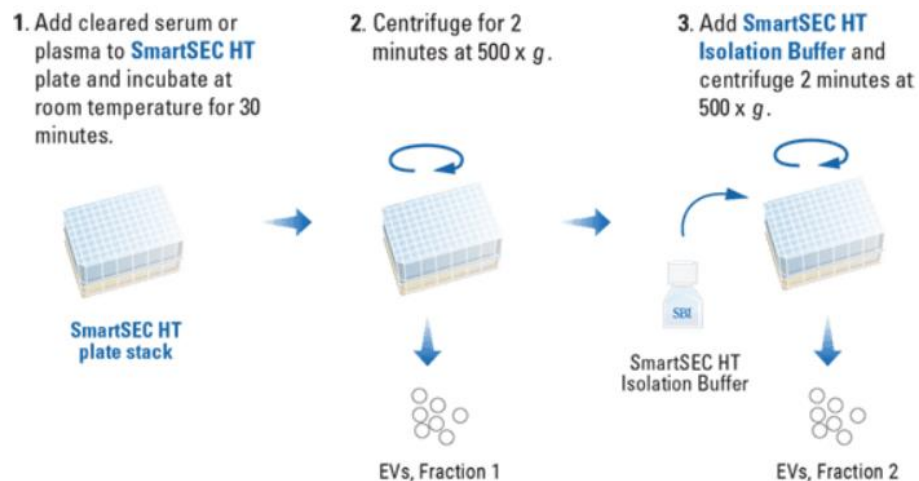


Figure 8. Workflow SmartSEC[™], plasma is incubated at room temperature for 30 min on the resin, 2 EV fractions are collected with centrifugation

Note. Acquired from System biosciences (2021). SmartSEC[™] HT EV Isolation System for Serum & Plasma. System Biosciences, LLC [Website]. Consulted on 7 April 2022 via [SmartSEC[™] HT EV Isolation System for Serum & Plasma | System Biosciences](#)

First the sealing on the wells necessary for performing the analysis was removed with a scalpel. Then the plate was spun at 500 g for one minute to remove the storage buffer. Five hundred μ L of SmartSEC Isolation Buffer was added in the wells to wash the resin. The stack was centrifuged again with the same settings. Five hundred μ L of PFP was added and incubated for 30 minutes at room temperature. The first

fraction was collected by spinning the plate stack at 500 g for two minutes. Then the second fraction was collected by adding 500 μ L of SmartSEC Isolation Buffer to the used wells and spinning the stack again at 500 g for two minutes. These fractions were stored at -80 °C in LoBind® Eppendorf tubes until further use.

4.3 Cell culture and EVs

4.3.1 Cell cultivation

The NCI-H1975 adherent human epithelial NSCLC cell line, containing the *EGFR* T790M mutation, was grown in 15–20 mL Gibco RPMI-1640 medium containing GlutaMAX™ supplemented with 10% FBS (Thermo Fisher Scientific). During culture, cells were incubated at 37 °C in 5% CO₂ and 95% relative humidity in a Binder incubator. On Mondays, 8.5×10^5 , and Fridays, 1×10^6 cells were passaged to new T75 cm² tissue culture-treated cell culture flask from Corning. Living cells were counted with a NucleoCounter® from Chemometec.

4.3.2 Cell EV production

For EV production, 11 330 500 cells in 200 mL Gibco RPMI-1640 medium containing GlutaMAX™ supplemented with 10% FBS were transferred to a 1000 cm² CELLdisc™ flask with four layers made from polystyrene (Greiner) between passage 14 and 17. After three days the 10% FBS medium was removed. The cells were washed with 80 mL PBS without Ca²⁺ and Mg²⁺. Then 120 mL Gibco medium containing GlutaMAX™ and 2% EV-depleted FBS (Gibco) filtered through a Steritop-GP, 0.22 μ m pore size filter was added.

After 24 hours the medium was collected and placed in 50 mL centrifugation tubes of Corning. The tubes were put through four consecutive differential centrifugation steps to remove cell debris and large vesicles, as displayed in Figure 9. After each centrifugation step, the formed pellet was discarded, and the supernatant was transferred to a new tube.



Figure 9. Removal of unwanted debris by centrifugation

The processed medium from this last step was used to collect cell EVs (4.4 NCI-H1975 EV Preparation).

4.4 NCI-H1975 EV preparation

The EVs from conditioned media of the NCI-H1975 cell line were prepared using two different EV separation workflows: SEC combined with ultracentrifugation and ultracentrifugation in itself were used.

4.4.1 SEC and ultracentrifugation

All the collected media were transferred to an ultrafiltration Centricon Plus-70 Centrifugal Filter made by Millipore and centrifugated at 3500 g for 10 minutes, 60 mL per spin for two times. When the sample had passed through, the column was spun again upside down to elute the concentrated sample. After this step, qEV SEC (paragraph 4.2.1) was used to collect the EV fraction of the medium. The first four fractions were pooled and transferred to polypropylene open top ultracentrifugation tubes. These tubes were placed in the Optima XPN-80 ultracentrifuge (Beckman Coulter) at 100 000 g in an SW 55 Ti rotor for three hours at 4 °C. All supernatant was discarded, and the formed EV pellet was resuspended in 500 µL of 0.1 µm filtered PBS. Aliquots of 10 µL were made and stored at -80 °C until further use.

4.4.2 Ultracentrifugation

For ultracentrifugation 16.5 mL of the collected medium was immediately transferred to 17 mL open top polypropylene ultracentrifugation tubes and centrifuged at 10 000 g for 30 minutes at 4 °C. Centrifugation was executed with a SW 32 Ti rotor. The supernatant was transferred to a new ultracentrifugation tube and centrifuged at 100 000 g for one hour and five minutes at 4 °C (Figure 10). After this step the medium was discarded, and the formed EV pellet was resuspended in 500 µL 0.1 µm filtered PBS. All separated EV samples were divided in aliquots of 10 µL and stored at -80 °C until further use.



Figure 10. Ultracentrifugation steps the collected cell medium undergoes to become EV stock

4.5 EV characterization

4.5.1 Western blot

The presence of different EV transmembrane proteins and contamination proteins in EV samples were detected with Western blot. To load samples in the gel a loading buffer was made of 900 µL 4x Laemmli loading dye mix (Bio-Rad) supplemented with 100 µL 2-mercaptoethanol (Bio-Rad). This mix colors the samples blue because it contains bromophenol blue. Ten µL loading buffer was added to 30 µL sample and heated for five minutes at 95 °C. A Mini-Protein TGX Stain-Free gel (Bio-Rad) was placed in the tank. Then the tank was filled with Tris/Glycine/SDS running buffer at a concentration of 25 mM Tris, 192 mM glycine and 0.1% SDS, (Bio-Rad). Thirty-five µL of sample was loaded per well of the stacking gel. To each gel a molecular weight ladder was added, called Precision Plus Protein™ WesternC™ Blotting Standards (Bio-Rad), which contains a predetermined set of size reference bands. Five µL was placed on the gel as reference for determining molecule size.

When all samples were loaded, the gel was run in a MINI-PROTEAN® Tetra System at 100 V until the samples were fully migrated into the gel. After, this voltage was

increased to 200 V. The run was stopped when the blue color reached the bottom of the gel. After electrophoresis the gel was taken out, and the top part and bottom-line were cut off. Then the gel was placed in 20% EtOH for five minutes for fixation of the proteins. After this step the gel was visualized on a Chemidoc platform (Bio-Rad) to see if the sample proteins were located in the gel. Next, the gel was placed in Milli-Q H₂O for five minutes. Before blotting 1x transfer buffer was added on the gel for five minutes. The transfer buffer is made by mixing 200 mL 5x transfer buffer (Bio-Rad) with 600 mL Milli-Q H₂O and 200 mL of pure ethanol.

For blotting the Bio-Rad Trans-Blot Turbo Transfer System was used. Filter paper was soaked in the transfer buffer and placed in the cassette. A nitrocellulose membrane was placed on top of this stack. On top of the membrane the gel was placed, and another stack of filter paper that was soaked was placed on top. The blot was run for 30 minutes at 1 A and 25 V and three minutes at 2.5 A and 25 V. After blotting, the gels were visualized in the Chemidoc to see if the proteins were transferred to the nitrocellulose membrane. The membrane was placed in blocking buffer. This was made with Regilait skimmed milk 0% fat by taking 2.5 g of milk powder and adding this in 50 mL of 1x PBS tween-20 (Thermo Fisher). The latter buffer, further called PBS-tween, was diluted from 20x to 1x in Milli-Q H₂O. The blot was blocked in this solution for one and a half hour. When the blocking was complete the blot was shortly washed in PBS-tween.

For specific protein detection, mouse anti-human primary antibodies were diluted in solution 1 for primary antibodies from SignalBoost™ Immunoreaction Enhancer Kit (Millipore) and added on the blot in a tray. The blot was developed at 4°C overnight. On the next day the blot was washed in PBS-tween for five minutes, this was executed 6 times. The secondary antibody was an anti-donkey mouse antibody conjugated with horseradish peroxidase for indirect detection. This antibody was dissolved in solution 2 for secondary antibodies from SignalBoost™ Immunoreaction Enhancer Kit, Millipore®. In this solution streptactin to visualize the used ladder was added, this component is called Precision Protein StrepTactin-HRP Conjugate from Bio-Rad. After one and a half hour the blot was washed in PBS-tween for five minutes, this was executed 6 times.

Amersham ECL Prime Western Blotting Detection Reagent was used to visualize the blots by chemiluminescence. Solution A and B are added in equal parts and the blot was placed in this liquid for five minutes. The presence of the antibody-bound protein could be seen on the Chemidoc platform as a noticeable band of the known protein size. An example of this is shown below in Figure 11. Cell lysate is used as positive control for CD9, and Cell medium is used as negative control for this protein. The positive control for apolipoprotein A1 is Cell medium, which contains serum and the negative control is cell lysate. The molecular weight of CD9 is 22-26 kDa and Apolipoprotein A1 is 30 kDa.

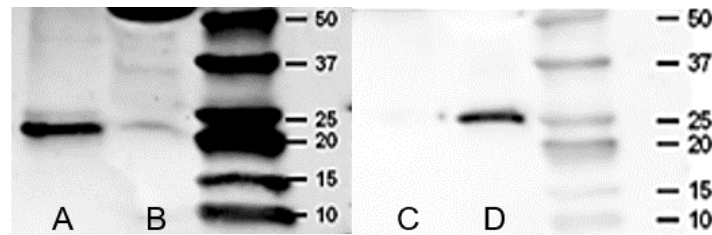


Figure 11. Example of positive and negative reaction western blot (CD9 left, Apolipoprotein A1 right).

A: Cell Lysate is positive for CD9 **C:** Cell lysate does not contain APO-A1
B: Cell medium does not contain CD9 **D:** Cell medium is positive for APO-A1

4.5.2 Nanoparticle tracking analysis

Using nanoparticle tracking analysis (NTA) one can measure the size distribution and concentration of particles present in a solution. These analyses were done on a Particle Metrix ZetaView® instrument. Before each measurement the device was calibrated with 100 nm polystyrene microspheres from Particle Metrix. Between different samples and solutions, the device was rinsed with Milli-Q H₂O.

Two different types of analysis were used to quantify the measured samples. Scatter measurements visualize all particles present in a sample, this also includes proteins etc. The optimal number of particles for quantification is 50 to 200 particles per frame. To find out the EV amount in a sample a fluorescent measurement was performed. This was done with CellMask™ Green plasma membrane stain (CMG, Invitrogen, Thermo Fisher Scientific), which is a fluorescent dye that visualizes EVs or membrane particles by intercalating in membrane structures. With a 488 nm wavelength fluorescent light filter inside the device this molecule was visualized.

The CMG was diluted 1/100 in 0.1 µm filtered PBS. Two µL of CMG was incubated for one hour at room temperature with 1–8 µL EVs depending on the concentration, making a total volume of 10 µL by adding 0.1 µm filtered PBS. A good concentration for analysis was chosen with a preliminary scatter measurement. The dilution of a sample that gave 250 to 300 particles per frame was incubated for the fluorescent measurement. After incubation 990 µL of Milli-Q H₂O was added and one milliliter of sample was injected in the device for examining particle size and concentrations.

4.5.3 Protein concentration determination

The protein concentration present in EVs fractions from PFP was determined using the Micro BCA™ Protein Assay Kit (Pierce Biotechnologie, 2022). Protein standards were diluted from an albumin stock vial to prepare a standard curve. The absorbance of these standards was used to calculate the unknown amount in a sample by linear interpolation. This can be done by using the equation describing the relationship between the measured absorbance and concentration (Figure 12). The absorbance was measured on the CLARIOstar plus plate reader (BMG Labtech) at 562 nm.

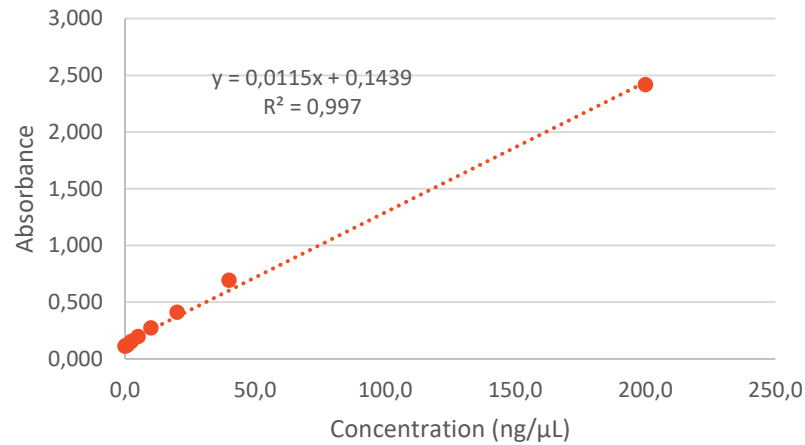


Figure 12. BSA standard curve

4.5.4 High-sensitivity flow cytometry

The produced NCI-H1975 EV stock was analyzed by high-sensitivity flow cytometry for the presence of CD81, CD9 and CD41 membrane proteins. To make this analysis possible the EV stock was diluted to a concentration of 1.25×10^9 particles/100 μL . These EVs were incubated with 20 μM carboxyfluorescein diacetate succinimidyl ester (CFDA) Cell Tracer (Invitrogen), for one hour in the dark at room temperature. This cell permeable component diffuses into the cell, where it is cleaved by intracellular esterases, by interacting with cellular amines via its succinimidyl groups to generate a highly fluorescent green dye that is impermeant to the cell membrane. This fluorescence is measured in the fluorescence channel at B530/30-A.

Next, 0.5 μg PE-Cy7 labelled antibodies against CD81, CD9 or CD41 (BioLegend) were added. Before adding the antibodies, antibody aggregates were removed by centrifugation at 17000 RPM at 4 $^{\circ}\text{C}$ for five minutes. These samples were incubated for one hour in the dark. Afterwards, PBS was added to an end volume of 300 μL .

The stained EVs were purified from excess of fluorescently labeled antibodies using Optiprep™ density gradient (STEMCELL Technologies) ultracentrifugation. For this gradient two buffers were made. The composition of Buffer 1 and Buffer 2 are listed in Table 1.

Table 1. Composition Buffers

Component	Amount in Buffer 1	Concentration in buffer	Amount in Buffer 2	Concentration in buffer
EDTA 100 mM stock	6 mL	6 mM	1 mL	1 mM
Sucrose	8.5573 g	0.25 M	8.5573 g	0.25 M
Tris-HCL	0.7268 g	60 mM	0.1211 g	10 mM
Milli-Q H ₂ O	To total 80 mL		To total 80 mL	

With these two buffers different Optiprep™ concentrations of 10, 30, 40 and 60% were made. These compositions are in Table 2.

Table 2. Working solutions needed amounts for 6 samples

% Optiprep™	Volume from 60% stock flask (mL)	Volume from 40% solution (mL)	Buffer 1 volume (mL)	Buffer 2 volume (mL)
60	7.000	/	/	/
40	8.000	/	4.000	/
30	/	3.750	/	1.250
10	/	3.250	/	9.750

The sample was added in 1.0 mL of 60% Optiprep™ in an ultracentrifugation tube and pipetted up and down until mixed. A gradient was made by carefully pipetting 700 μ L of 40% on top of the 60% solution. Then 700 μ L of 30% Optiprep™ was added. The final layer was two milliliters of the 10% solution. The tubes were placed in the ultracentrifuge at 367 600 g on 4 °C for approximately 16 hours. After centrifugation 10 fractions of 480 μ L were collected and vortexed. The produced fractions were measured by Berckmans P. on the BD FACSymphony™ A1 high-sensitivity flow cytometer (Becton Dickinson) using in-house validated procedures.

In the flow cytometer all particles from a sample were visualized in dot plot showing B530/30-A fluorescence intensity as function of small particle side scatter (SP-SSC). Based on this, a gating strategy for CFDA⁺ events was implemented for identifying EV particles (Figure 13A, gate C++). In this CFDA⁺ gate another gating takes place for events fluorescently labeled with antibodies against CD9, CD81 or CD41. These are represented in dot plots showing YG780/60-A fluorescence intensity as a function of SP-SSC (Figure 13B and C, gate A++). Figure 13B shows control of EVs stained with CFDA but without antibody labeling, in Figure 13C the signal of EVs with CFDA and PE-Cy7-conjugated CD9 antibodies is visible.

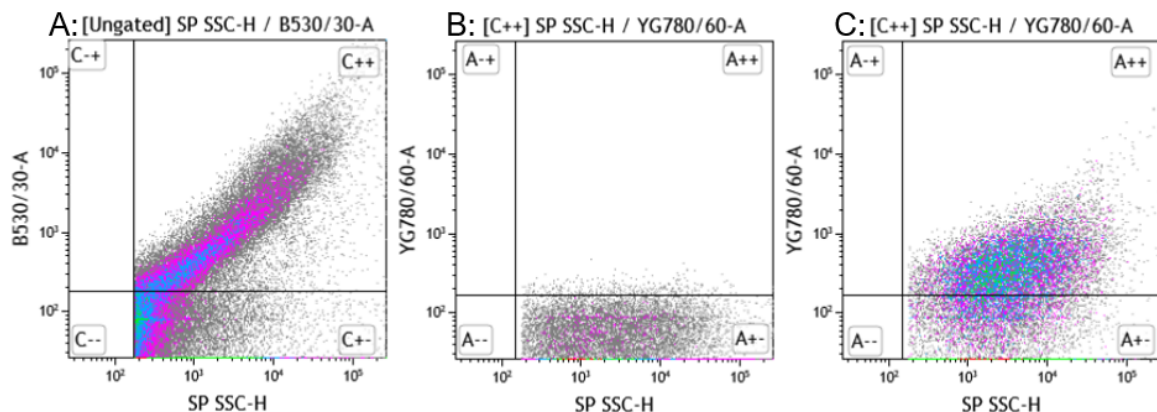


Figure 13. Signal flow cytometry. **A:** CFDA positive particles and background signal, **B:** Signal for PE-Cy7® with no AB in CFDA positive particle group, **C:** Signal for PE-Cy7® with CD9 AB

4.5.5 Bio-layer Interferometry

Bio-layer Interferometry measurements were done using the Octet® K2 (Sartorius) device. In these measurements two octet® streptavidin (SA) conjugated (Sartorius) tips were used. An antibody of choice can be conjugated with a biotin link. Biotin-labeled mouse anti-human antibodies (BioLegend) against the tetraspanins CD9 and CD81 a concentration of 100 µg in 200 µL were used. A non-epitope binding isotype control antibody was used on the other SA tip. This Isotype control is a Biotin Mouse Ig G1 antibody made by BioLegend.

A kinetics buffer solution was used in this analysis, 10x kinetics solution (Sartorius) is diluted in 0.1 µm filtered PBS to a 1x concentration. This is performed in a low-bind polypropylene 96-well plate (Greiner), with each well containing 200 µL of selected solution. The measurement can be divided into a chosen number of steps.

Before starting a measurement, the SA tips were hydrated in the 1x kinetics PBS solution for 10 minutes. The EV binding analysis consisted of 5 steps in total. Step 1 was a baseline step of 360 seconds, during which the signal of the tip in kinetics buffer is measured. In Step 2 the tips move to a new well. This contained the chosen antibodies in the kinetics buffer solution with a concentration of 1/200 to allow antibody conjugation on the tip, step 2 takes 600 seconds. The third step consisted of another baseline in a new well with kinetics buffer for 300 seconds, the purpose of this baseline was to remove excess antibodies and give a reference point for signal variation. In the next well (step 4), EVs were added in a chosen concentration which lasted 7200 seconds. Step 5 included a washing step of 300 seconds and was implemented to remove non-specifically bound EVs from the tips in a well with kinetics buffer.

When the tips were removed from the Octet®, they were placed in a LoBind® protein Eppendorf tube containing 20 µL of 0.1 µm filtered PBS. The tubes were placed in an Eppendorf ThermoMixer F1.5 at 100 °C, 700 RPM for 30 minutes to lyse the bound EVs. Next, the tubes were spun down shortly in an ELMI FugaMIX™ microcentrifuge and placed in a -80 °C to serve as sample for ddPCR analysis.

An extra EV capture validation was performed with 50 nm spherical gold nanoparticles (Nanopartz™). These gold nanoparticles carry streptavidin molecules at their surface. A biotin-conjugated antibody can be covalently bound to these nanoparticles. Conjugation was performed by adding an excess quantity of 6 µL CD9 to 100 µL Au nanoparticles, followed by overnight incubation at 4°C with agitation.

To remove excess unbound antibodies from the gold nanoparticle-antibody conjugates, 1,5 mL PBS was added, and the solution was vortexed. This volume was spun five times on 20627 g at 4°C. The supernatant was discarded (+- 1,2 mL) and replaced with fresh PBS before every new spin. At the last spin no new PBS was added, and the maximum possible supernatant was removed, this method produced ±200 µL solution of CD9-coupled Au. These particles were used in a BLI-EV measurement, 1/10 of this solution was diluted in kinetics buffer and added in the gold sandwich assay.

The conjugated particles were measured on the Nanodrop device and showed the following spectrum (Figure 14). The peak value was at 529 nm with an absorbance of 0,227.

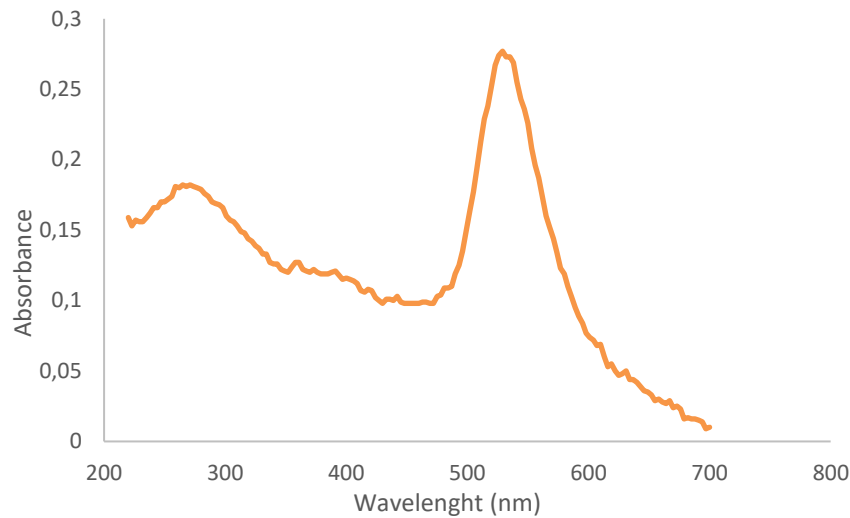


Figure 14. Spectrum of Au nanoparticles conjugated with CD9

The anti-CD9 conjugated Au nanoparticle stock concentration was the following:

$$c_{Au\ nanoparticle} \left(\frac{mol}{L} \right) = \frac{A}{\epsilon \times l} = \frac{0,277}{1.51 \times 10^{10} M^{-1} cm^{-1} \times 0.10 cm} = 1.8 \times 10^{-10} mol/L$$

$$\begin{aligned} c_{Au\ nanoparticle} \left(\frac{particles}{L} \right) &= c_{Au\ nanoparticle} \left(\frac{mol}{L} \right) \times avogadro\ constant \\ &= 1.8 \times 10^{-10} \frac{mol}{L} \times 6.022 mol^{-1} = 1.1 \times 10^{14} Au\ nanoparticles/L \end{aligned}$$

This means that $1,1 \times 10^{13}$ Au nanoparticles/L were used in the sandwich assay.

4.5.6 ddPCR

Sample analysis with ddPCR is possible after converting the sample pool into droplets. These droplets were made with the droplet generator device (Bio-Rad). For analyzing the captured amount EV-DNA on the BLI SA tips, 4 μ L sample solution from the 20 μ L solution (4.5.5 BLI) was added in 18 μ L of ddPCR master mix. The used composition of master mix is noted in Table 3.

Table 3. Master Mix composition

Component	Amount (μ L) \times samples + 2
2x ddPCR supermix for probes (no dUTP) (Bio-Rad $\text{\textcircled{C}}$)	11
20x primers and probes (ddPCR Mut Assay, VAL EGFRT, T790M, Hsa fam/hex) (Bio-Rad $\text{\textcircled{C}}$)	1.1
RT-PCR Grade H ₂ O (Invitrogen)	X (x = 9.9 - sample volume)

A volume of 20 μL of master mix with sample was converted into droplets by adding this volume and 70 μL oil into the droplet generator. The formed droplets were collected and placed into a PCR plate. When all the sample droplets were collected in the plate, it was sealed. A PCR procedure was implemented (Figure 15).

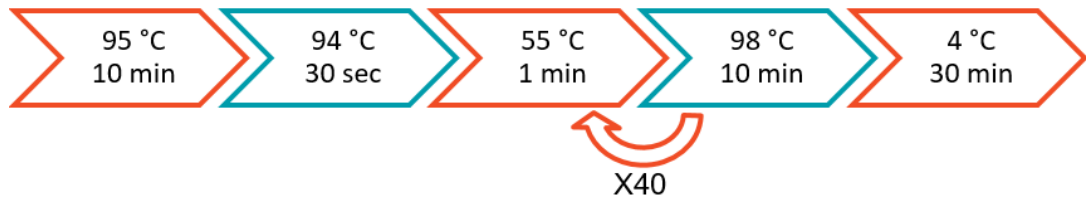


Figure 15. PCR cycle steps

After the full cycles the samples were placed at 4 °C for 30 minutes to stabilize the droplets. After the 30 minutes the plate was placed in the droplet reader and collected data was analyzed in the QuantaSoft™ analysis pro application (Bio-Rad, 2022). The QuantaSoft™ analysis pro application calculates concentrations based on detected positive droplets. Thresholds needed to be set, to confirm when droplets contain the investigated mutation, when they contain the wild-type DNA and when they contain nothing (Figure 16).

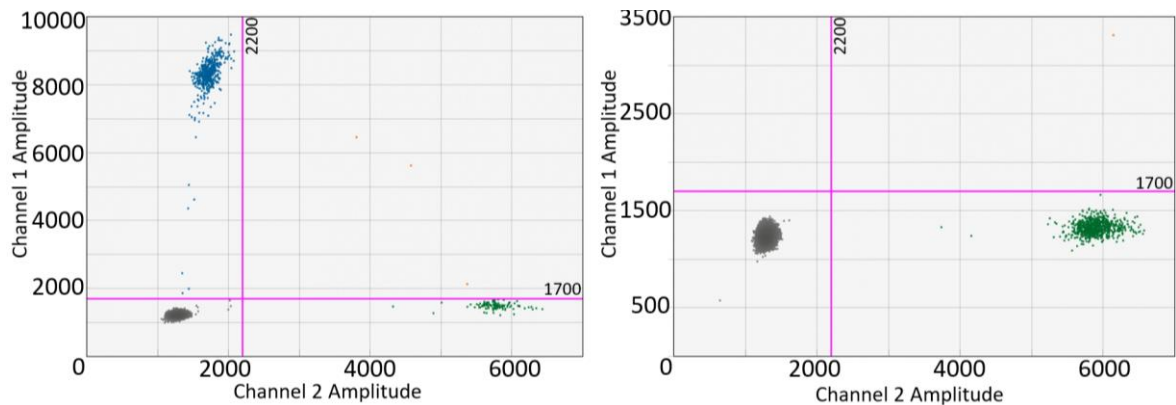


Figure 16. Used thresholds for data analysis (channel 1: 1700, channel 2: 2200), the limits were placed with the help of positive (containing mutation, represented as blue area on left graph) and negative (containing wild-type DNA, represented as green area on right graph) controls

The analyzed droplet signals of samples that fall in the selected area were containing the DNA mutation, the selected area is the upper left quadrant. The lower left quadrant contains empty droplets, these give no signal. Inside the lower right quadrant is the wild-type DNA containing droplets. The upper right quadrant shows droplets that are double positive, these contain mutation and wild-type DNA.

5 Results

The main goal of this work is to study potential advancements in NSCLC diagnostics, by the optimization of detection of the *EGFR* T790M mutation in EVs. Firstly, the influence of two different blood collection tubes on EV concentration, EV protein type and concentration were analyzed. Secondly, an application was developed for capturing of EVs on a bio-layer Interferometry platform and subsequent DNA mutation analysis by ddPCR.

5.1 Effect of blood collection tubes on the EV fraction

The influence of two blood collection tubes (BCTs) on the EV fraction, protein concentration and presence of protein markers was evaluated. This by creating PFP on the day of blood collection and five days after collection. The isolated plasma-derived EV samples were characterized using protein concentration determination, western blotting and high-sensitivity flow cytometry.

5.1.1 Protein analysis

Total protein contents of the PFP EV fractions after SEC was calculated. The PFP that was created on the day of collection and five days after collection was investigated. As can be seen in Figure 17, the total protein concentration remains consistent in both tubes if left for multiple days. The first four fractions produced with a qEV sample clearing step were used in this analysis. Protein concentration increases with fraction number. This means that the higher the fraction number the more protein contaminants are mixed in with the EVs.

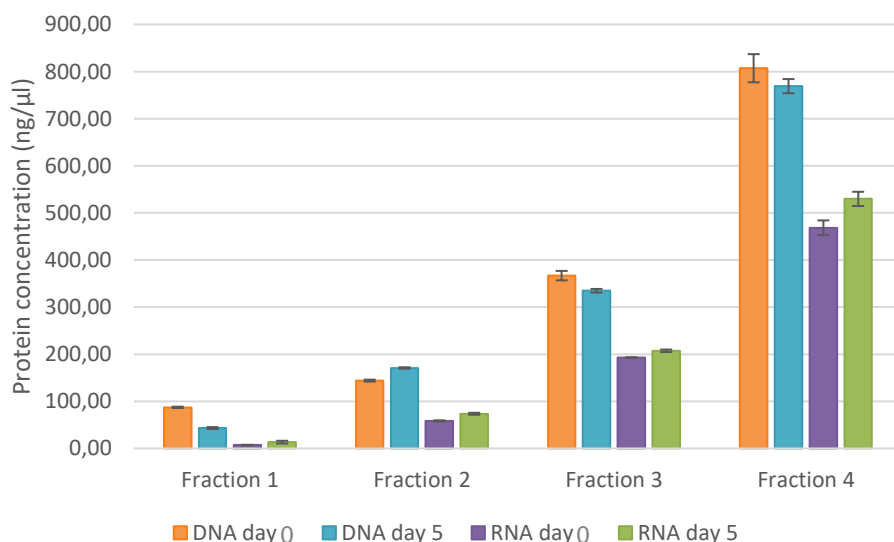


Figure 17. Protein contents in the first four collected qEV fractions of cell-free DNA(DNA) and RNA Complete (RNA) tubes compared on different isolation day measured in duplicate

The variation between storing the sample for five days and direct manipulation is visualized in Figure 18. The total protein concentration seems to remain stable over different plasma preparation moments.

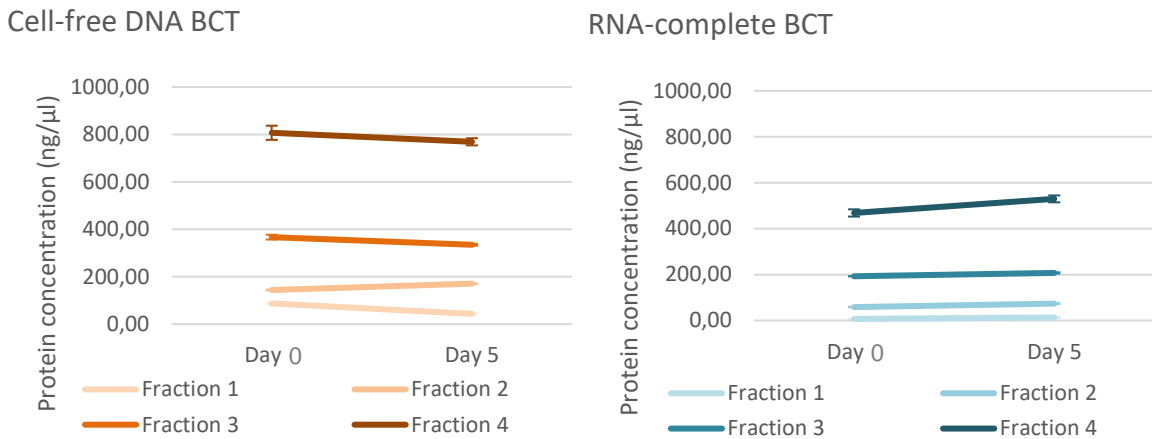


Figure 18. Change in protein concentration between the different manipulation dates measured in duplicate

Donor variation was also compared, three different donors and their total protein concentration in plasma qEV fractions were measured with the μ BCA kit (Figure 19). The concentrations were calculated with the standards graph in Figure 12.

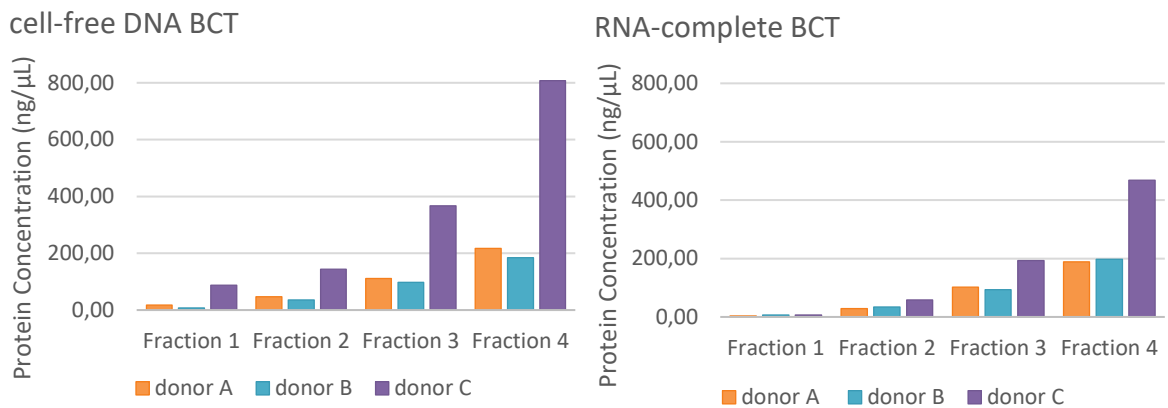


Figure 19. Donor protein concentration in the different qEV produced fractions: left cell free DNA tube plasma after qEV, right RNA tube plasma after qEV

The protein contents can vary largely between different donors (Figure 20). The DNA BCT (Cell-free DNA BCT) qEV fractions contain more protein on average than the RNA BCT (RNA Complete BCT) qEV fractions.

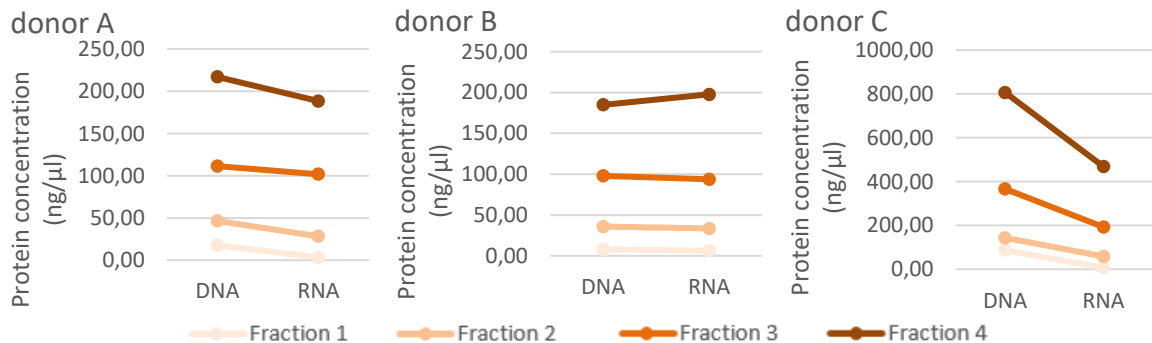


Figure 20. Comparing protein concentration between cell-free DNA tube and RNA tube, and variance between three different donors

Besides qEV, SmartSEC was used for EV isolation on PFP of donor A and B, collected in the two BCT types. The two produced SmartSEC fractions were also analyzed for total protein content (Figure 21).

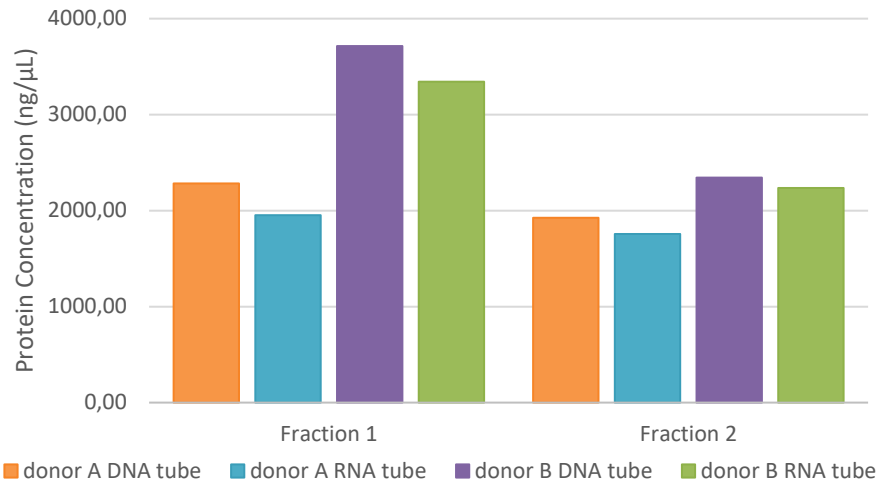


Figure 21. Donor protein concentration variation in Smart SEC fractions

SmartSEC fractions contain more total protein per fraction than the qEV fractions, this could be caused by the fraction number. The qEV SEC method produces 13 fractions from 500 μ L plasma sample while SmartSEC only produces two fractions from the same sample volume. The cell-free DNA BCT contains more protein in total than the RNA BCT in these fractions (Figure 22).

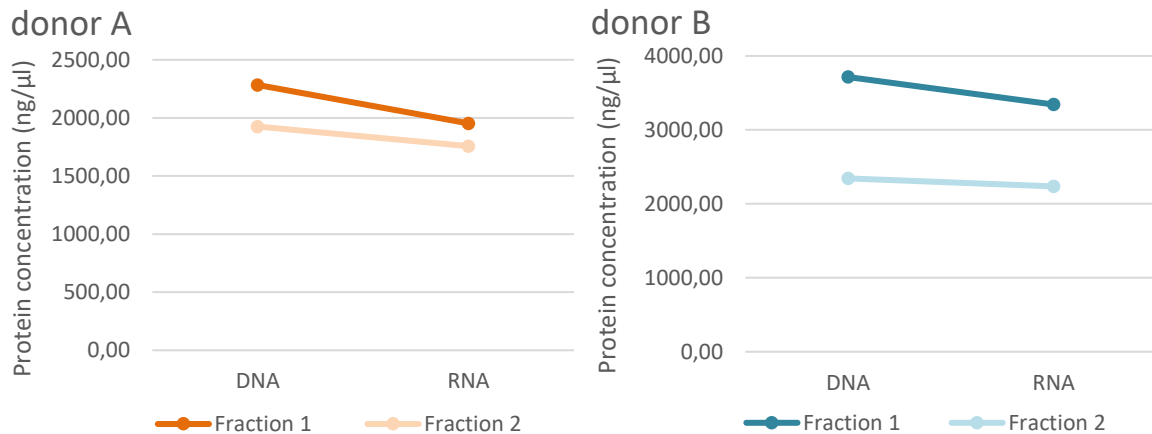


Figure 22. Comparing DNA and RNA tube SmartSEC fractions: left donor A, right donor B

The obtained EV fractions from the cell-free DNA and RNA BCT were also analyzed for presence of protein markers in the first four qEV fractions and both SmartSEC fractions, 35 μ L of the obtained fractions was placed on western blot. Unconditioned medium was used as a negative EV control and NCI-H1975 cell lysate was used as a positive control for EVs. The protein markers tested on the SEC fractions were CD9, a EV specific tetraspanin, Calnexin, an integral protein of the endoplasmic reticulum, apolipoprotein A1, a lipoprotein of plasma, and CD41, a platelet EV-specific marker (Figure 23).

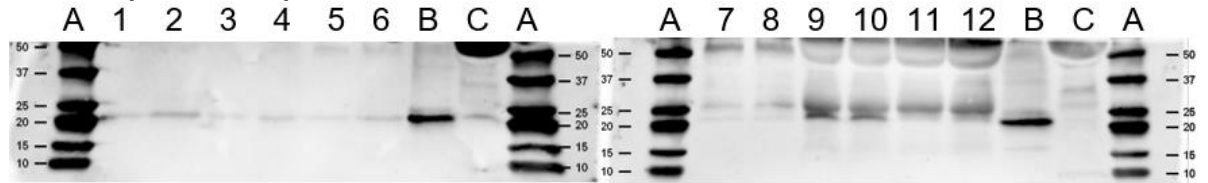
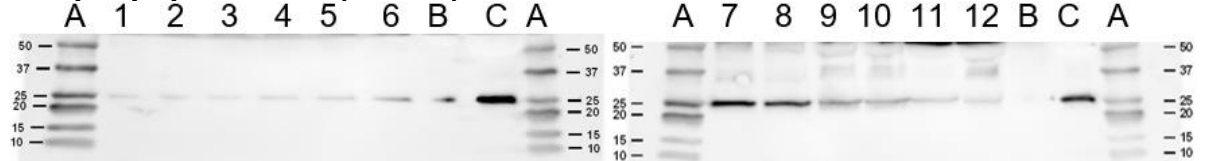
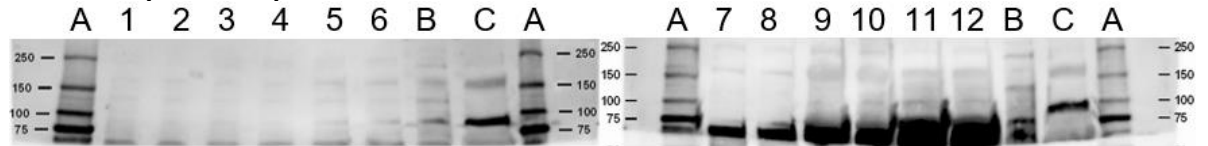
A. CD9 (22-26 kDa)**B. Calnexin (90 kDa)****C. Apolipoprotein A1 (30 kDa)****D. CD41 (113 kDa)**

Figure 23. Western blot of EV protein marker CD9 (**A**), non-EV protein marker calnexin (**B**), lipid-protein complex marker apolipoprotein (**C**) and platelet marker CD41 (**D**). Lane numbers and explanation:

- | | | |
|--------------------|----------------------|-----------------------|
| 1: DNA qEV1 | 6: RNA qEV3 | 11: DNA SMS 2 |
| 2: RNA qEV1 | 7: DNA qEV4 | 12: RNA SMS 2 |
| 3: DNA qEV2 | 8: RNA qEV4 | A: Ladder |
| 4: RNA qEV3 | 9: DNA SMS 1 | B: cell lysate |
| 5: DNA qEV3 | 10: RNA SMS 1 | C: cell medium |

(DNA: Cell-free DNA BCT plasma, RNA: RNA Complete BCT plasma)

CD9 was most visible in fraction 1–3 qEV and in fraction one of SmartSEC (Figure 23). Therefore, these fractions were used to compare the influence of leaving the sample for five days on EVs. In the RNA Complete BCT PFP qEV fraction one CD9 seems the most prominent. Calnexin was absent in the fractions of PFP, this means that there are no cell residues. Apolipoprotein A1 is a blood protein, the density of this protein band increases with fraction number of qEV and is abundant in SmartSEC fraction one. The platelet EV marker CD41 was absent in these fractions, no detectable platelet EVs are present as contamination in these fractions.

The amount of calnexin and CD9 was compared between the samples that were stored for five days, and the directly produced PFP produced (Figure 24).

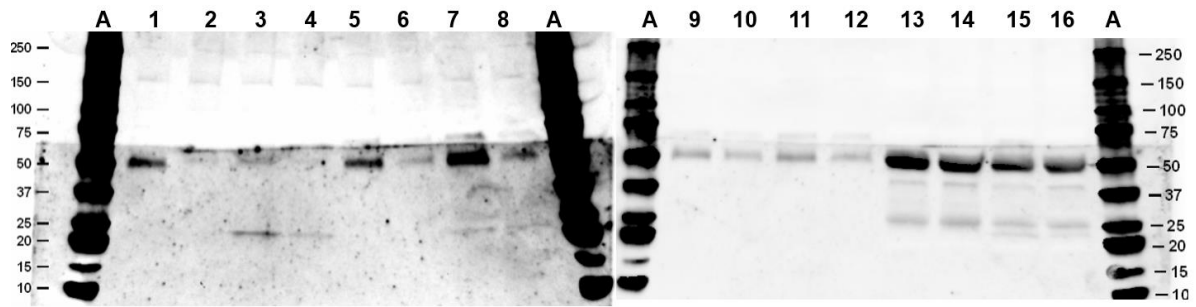


Figure 24. Western blot analysis of Calnexin (90 kDa, top) part and CD9 (22-26 kDa, bottom) in EV isolates. Left blot: qEV fractions 1 and 2, Right blot: qEV fraction 3 and SMS fraction 1. Lane numbers and explanation:

1: DNA qEV1 at day 1 6: RNA qEV2 at day 1 11: DNA qEV3 at day 5 16: RNA SMS1 at day 5
 2: RNA qEV1 at day 1 7: DNA qEV2 at day 1 12: RNA qEV3 at day 5 A: ladder
 3: DNA qEV1 at day 5 8: RNA qEV2 at day 5 13: DNA SMS1 at day 1
 4: RNA qEV1 at day 5 9: DNA qEV3 at day 1 14: RNA SMS1 at day 1
 5: DNA qEV2 at day 1 10: RNA qEV3 at day 1 15: DNA SMS1 at day 5

(DNA: Cell-free DNA BCT plasma, RNA: RNA Complete BCT plasma)

No calnexin was present in the sample, the purification methods remove these residues efficiently. In qEV fraction one of the cell-free DNA tube after five days is CD9 the most noticeable. This tetraspanin seems to be present in both the blood collection tubes after five days, qEV fractions one and two.

5.1.2 High-sensitivity flow cytometry

Extracellular vesicle stability in the tubes was evaluated at day one of PFP production by measuring qEV SEC fraction two of this plasma with flow cytometry. This was implemented after incubation with PE-Cy7[®] labeled antibodies against EV markers. In the flow cytometry analysis, the EVs were identified using CFDA. The presence of a marker on the EV population was calculated against these CFDA positive particles.

The EV population in the DNA BCT consisted of 9-18% of all particles in the used fraction. In the RNA BCT the EV population consisted of 29-67% of all particles in the used fraction (Table 4). The formula used to calculate particles/mL in the qEV fraction two sample of both BCTs was used as follows.

$$c \text{ in particle/mL} = \frac{\text{particles measured in 60 sec (particles/min)}}{\text{Sample flow } (\mu\text{L/min)}} \times 10^3$$

Table 4. EV quantities in Cell-free DNA BCT (left table) and RNA BCT (right table) qEV fraction 2 measured on flow cytometer

Cell-free DNA tube				RNA tube			
Sample flow (μL/min)	Particles measured in 60 sec (1/100)		Sample flow (μL/min)	Particles measured in 60 sec (1/200)			
	ALL	CFDA		ALL	CFDA		
Average of 3 repetitions	2.8	91526	16453	Average of 3 repetitions	3.5	43800	17587
SD	0.35	4765	696	SD	0.16	3696	651
c in particles/mL		3.3×10^9	5.9×10^8	c in particles/mL		2.5×10^9	1.0×10^9

The collection of measured data is in Attachment 3 and Attachment 4.

The RNA BCT stabilized more EVs in the sample than the DNA BCT did. This was within the two different BCTs collected from one volunteer and processed on collection day to PFP. This CFDA positive population was evaluated on presence of three different markers. The marker that was most present in both tubes was CD 41, this is a platelet EV marker. The second most abundant marker was CD81 which is an EV membrane marker according to the MISEV guidelines. The marker present in lowest % of events was CD9 which is also an EV membrane marker according to the MISEV guidelines. An overview is displayed in Figure 25.

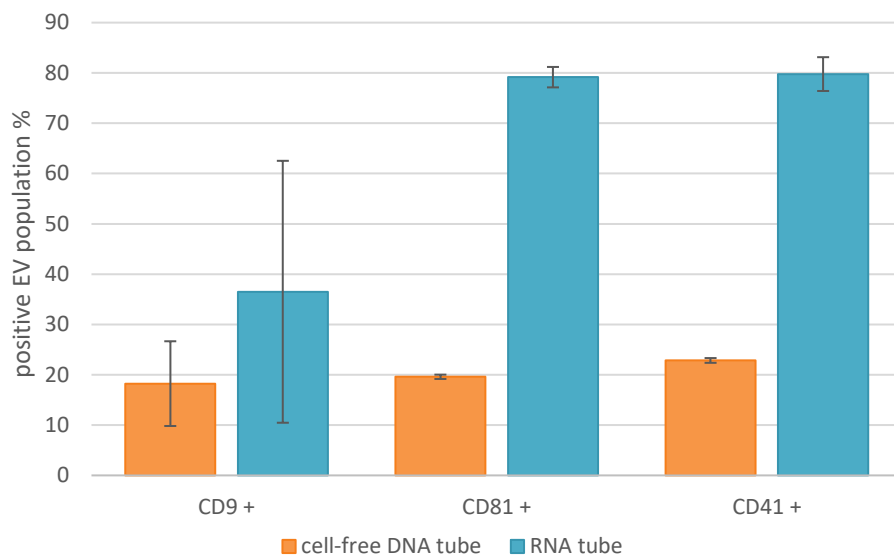


Figure 25. percentage of EVs in stock containing the markers: CD9, CD81 or CD41 measured in triplicate

The RNA BCT contains more CFDA positive particles than the DNA BCT. This means that there are more EVs available in this BCT. The CD9 and CD81 containing CFDA positive EVs are also more present in the RNA BCT. The platelet marker is higher as well, this means that a large part of the available EVs was produced by thrombocytes. However, these EVs are not useful for lung cancer EV-DNA mutation detection, because they are not produced by the lung cancer cells. In conclusion, the results presented here indicate that the RNA BCT is performing better in stabilizing PFP EVs originating from different cell types, compared to the DNA BCT.

5.2 Evaluation of DNA mutation detection in specific EV subpopulations captured by BLI

First the NCI-H1975 cell line-derived EV stocks were characterized to determine the concentration and size of EVs using fluo-NTA and for the presence of membrane proteins using flow cytometry. These were then used for the optimization of EV binding using BLI. The EV binding was optimized using both CD81 and CD9, a sandwich assay with gold-conjugated antibodies was performed, and captured EVs were release and lysed for analysis of mutational DNA content using ddPCR.

5.2.1 Characterization of NCI-H1975 cell line-derived EVs

Flow cytometry was used to determine the percentage of EVs exhibiting CD81 and CD9 on their membrane. Almost 60% of all EVs detected expressed CD9, and for CD81 this was 40%. Therefore, CD9 and CD81 were used for the optimization of real-time EV binding using bio-layer interferometry. The full collection of measurement results is in Attachment 5.

Fluorescent-NTA was used to determine the particle number concentration and size distribution of EVs present in the EV stock. Size distribution of the particles in both stocks is plotted in Figure 26.

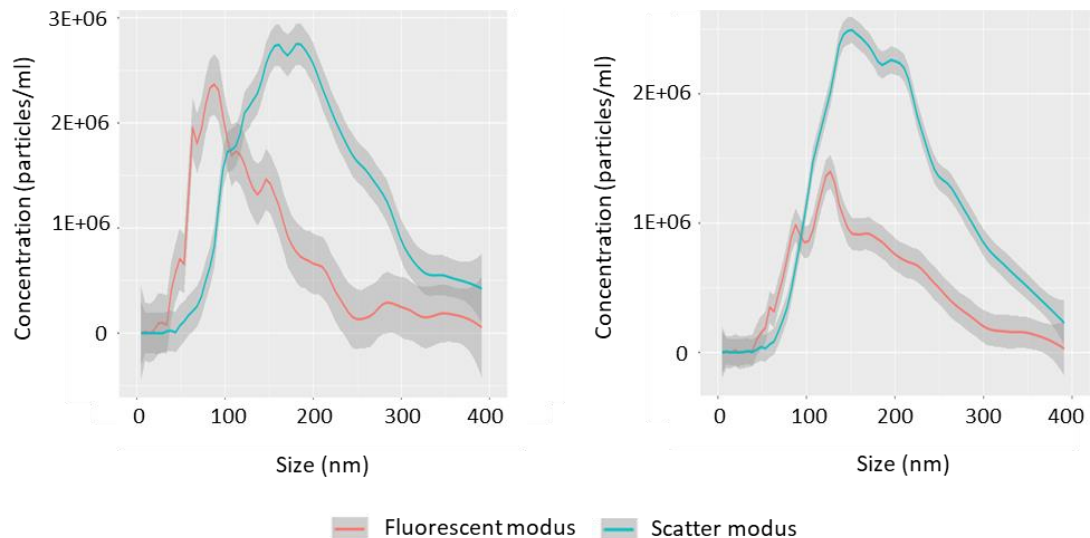


Figure 26. Particle number size distribution (particles/mL versus nm) of EV stocks to be used for BLI experiments with anti-CD9 (left) and anti-CD81 antibodies (right), measured in fluorescent modus and scatter modus using NTA.

The median size in fluorescent mode of the CD9 EV stock is 89.5 nm, the CD81 EV stock median is 119.3 nm. Measured stock concentrations are in Table 5, average and standard deviation were calculated. The concentrations of the two stocks were used for determining the concentration used in CD81 and CD9 BLI measurements.

Table 5. EV SEC+UC stock concentration

	EV stock used for CD9 (particles/mL)	EV stock used for CD81 (particles/mL)
1	3.5×10^{11}	2.3×10^{11}
2	3.8×10^{11}	2.0×10^{11}
3	4.0×10^{11}	2.2×10^{11}
gem	3.8×10^{11}	2.2×10^{11}
SD	2.5×10^{10}	1.5×10^{10}

Attachment 6 and Attachment 7 contain all the collected data.

5.2.2 Optimization of EV binding

Optimization of EV capture was performed by using anti-CD9 or anti-CD81 antibodies, these are general EV markers according to the MISEV guidelines (Attachment 1). Four different EV concentrations were used and made from the same EV stock solution. The stock volumes needed were calculated as in the example below.

$$V_{EV\ stock} = \frac{c_{used\ in\ BLI} \times V_{tot}}{c_{EV\ stock\ average}}$$

This formula was applied for all the volume and concentration calculations used in the BLI measurements (Attachment 8). The time kinetics and detected signal change during EV binding on the antibody-coated tips was plotted, all starting at 0 to enable comparison between different measurements (Figure 27).

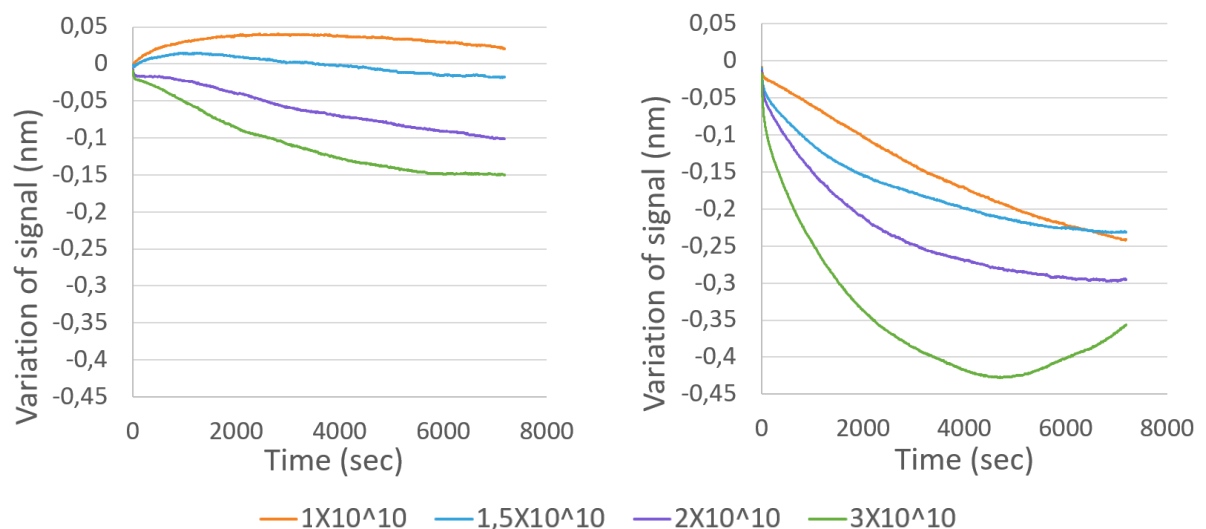


Figure 27. Influence of EV concentration on the time kinetic EV binding to anti-CD9 (left) and anti-CD81 (right) coated tips

The CD81 signal change is more prominent than the CD9 signal change. A visible correlation can be seen, the higher the concentration the more negative the overall signal. A linear correlation between signal and EV concentration was found at 3000 seconds into the EV binding phase, with the highest R^2 whilst still giving a high enough signal difference (Figure 28).

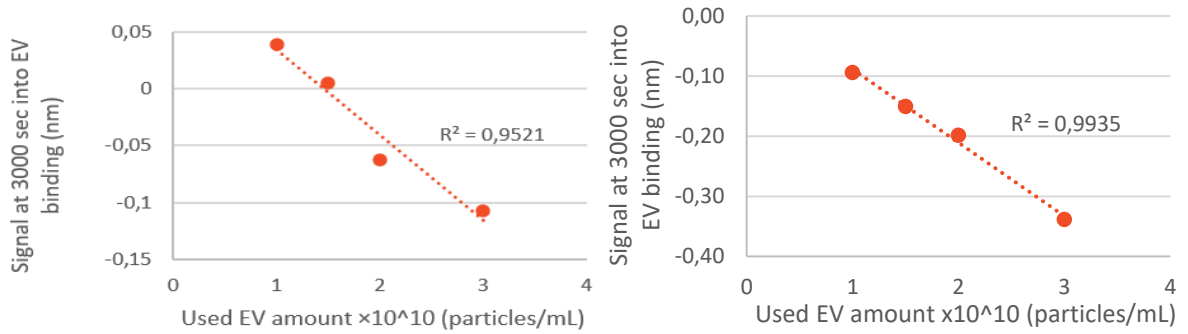


Figure 28. Linear relation between kinetic signal and particles/mL: left CD9, right CD81

The correlation between particle concentration and detected signal is more linear for CD81 tips than CD9 tips, and CD81 also shows a larger signal change.

The bound number of antibodies on the tip could have an influence on EV binding. There is a variation on the binding signal between the anti-CD9 and anti-CD81 antibodies that are bound on the tip (Table 6).

Table 6. Binding signal on BLI of antibodies before EVs are added

AB ligand	average of AB binding signal at end of step 2 (nm)	SD (nm)
CD9	3.875	0.042
CD81	4.143	0.095

When less antibodies are bound to the tip, less EVs can bind. This could have influenced the difference in signal intensity.

A fixed particle concentration of 2×10^{10} particles/mL was added on two different days, under the same conditions in a BLI measurement to evaluate measurement stability. Figure 29 shows the variation on signal change between these two measurements using anti-CD81.

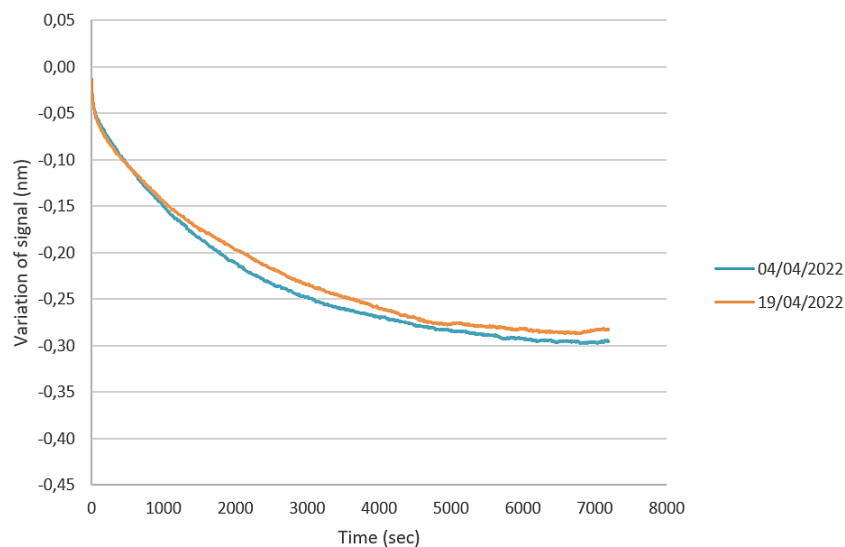


Figure 29. Stability test use of same EV stock and same concentration

At 3000 seconds of EV binding there is a percentile difference of 5.83% in EV signal, and 0.00819 as standard deviation.

5.2.3 Sandwich assay with anti-CD9 antibody conjugated gold nanoparticles

To make sure that the observed signal is the specific signal of EV binding, a sandwich assay was performed. The anti-CD81 antibody was conjugated to the tip while anti-CD9 was conjugated on gold nanoparticles. In this assay solely the EVs can contain both used markers and thus, only when an EV is captured in between both antibodies an extra signal change after adding the gold nanoparticles can happen.

First CD81 and an isotype control (IgG1) were bound on separate tips. Both these tips were put in wells containing the same concentration of EV particles in kinetics buffer. After EV binding the tips were washed in kinetics buffer for 300 seconds to remove excess EVs. When this step was finished the tips were placed in a gold nanoparticle containing suspension. The whole variation in detected signal is plotted in Figure 30.

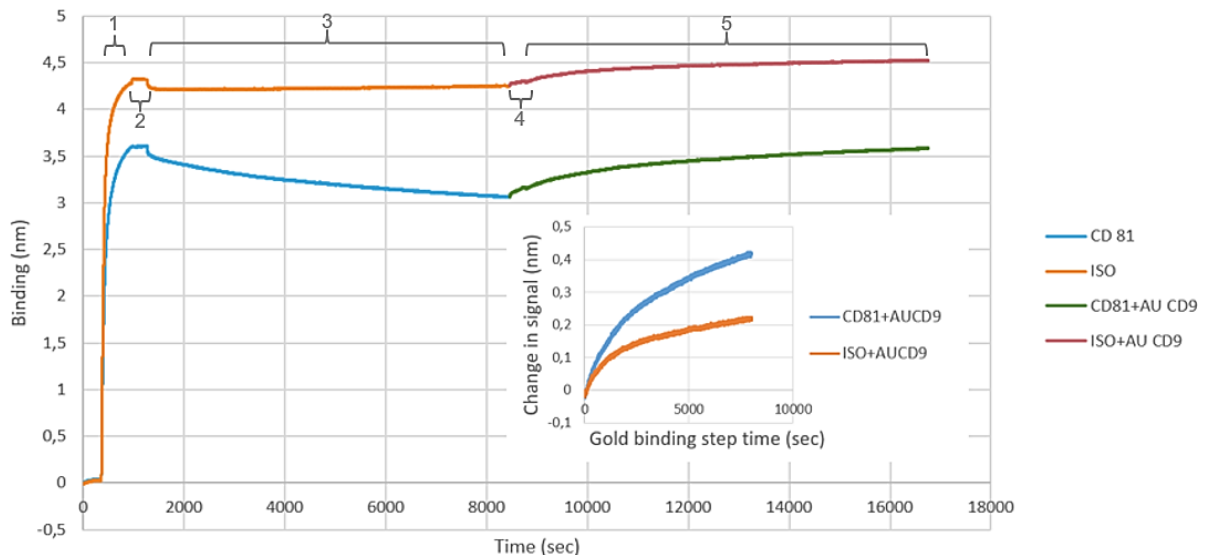


Figure 30. Confirmation of EV presence on SA tip: 1; binding of antibodies, 2; discarding excess antibodies, 3; EV binding, 4; discarding excess EVs, 5; conformation of bound EV presence with CD9 conjugated gold. The graph in the lower right corner shows the difference in binding signal of gold between the CD81 with EVs and the isotype with no EVs

There is a difference in signal between the CD81 tip and the isotype tip in step 5. The gold CD9-EV-CD81 sandwich signal is 0,20 nm higher than the isotype tip in gold solution. This measurement confirmed that CD81 captured EVs, and that IgG did not capture the same EV amount. From this it is possible to conclude that a downward signal means that EVs are being captured on the antibody-conjugated SA tip.

5.2.4 Downstream analysis of captured EV content

Using ddPCR analysis the content of tip bound EVs was analyzed. This was attempted by first trying to capture the NCI-H1975-derived EVs containing the *EGFR*

T790M mutation and then evaluating if this mutation could be detected on ddPCR. Anti-CD81 and IgG isotype control-conjugated tips were incubated with different concentrations of captured particles and assessed (Figure 31).

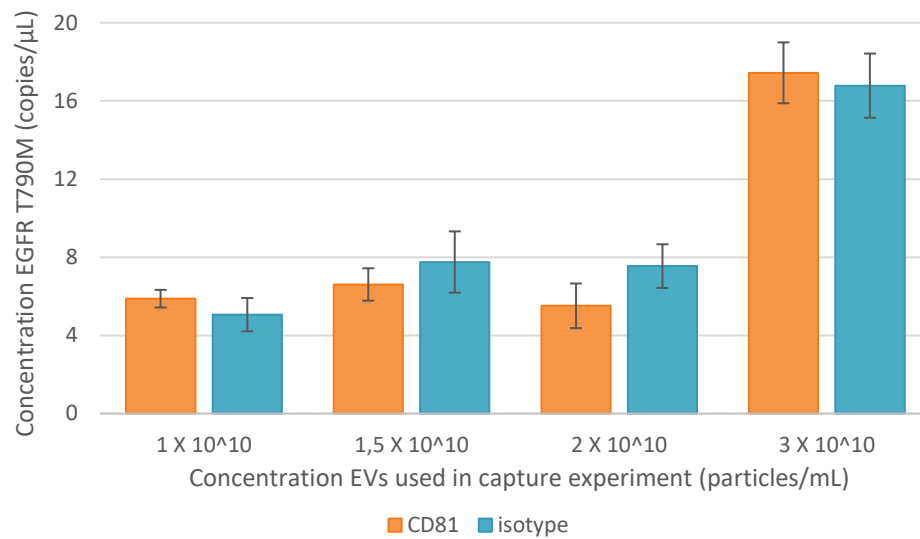


Figure 31. ddPCR results of CD81 and isotype BLI SA tips with different EV concentrations (EGFR T790M mutation analysis) measured in quadruple

An example of a ddPCR measurement of the captured EVs is plotted in Figure 32. The upper left quadrant shows the droplets containing the EGFR T790M DNA mutation. In the lower left quadrant are the empty droplets, the lower right quadrant shows wild-type DNA containing droplets.

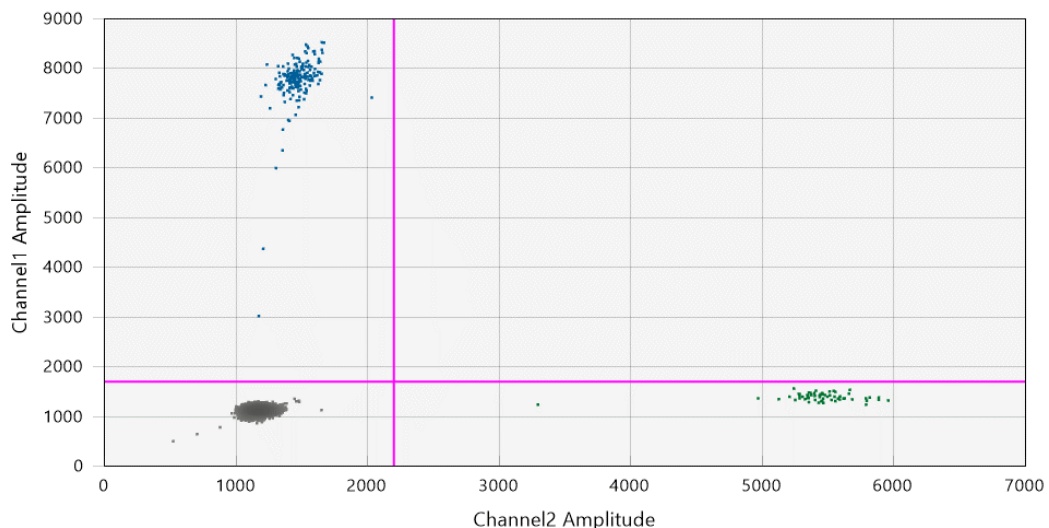


Figure 32. Plot of CD81 tip with 3 X 10¹⁰ EVs: upper left quadrant, positive for EGFR T790M droplets; lower left quadrant, empty droplets; lower right quadrant wild-type DNA containing droplets

There is no clear difference between used EV amount and ddPCR measured concentrations between the anti-CD81 and anti-IgG antibody conjugated tips. This was not the expected result, a correlation between mutation DNA copies and EV concentration was anticipated. Therefore, we tested the hypothesis that free DNA

fragments were present in the EV isolates and influenced the signal. This was done by submerging the IgG coated BLI tips in kinetics buffer with 40 ng/mL gBlock DNA fragments containing the *EGFR* T790M mutation Figure 33.

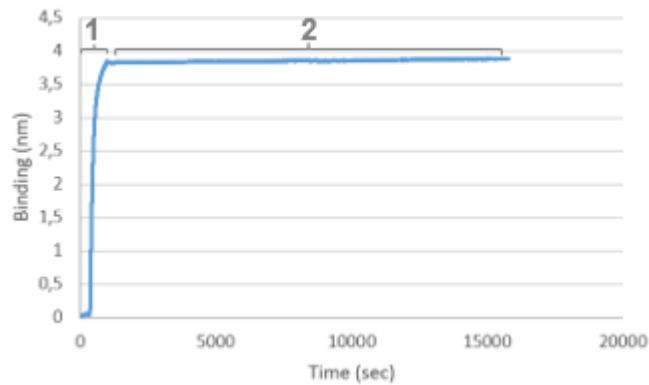


Figure 33. Detected BLI signal with IgG Isotype antibody coated tips in gBlock DNA fragments. Coating of the tip (part 1) and lowering the tip in 40ng/mL gBlock DNA fragments (part 2)

No visible large influence was observed during part 2 with gBlocks added, these tips were then also measured on ddPCR. Figure 34 shows that free DNA fragments can have an influence on the ddPCR measured mutant DNA concentration. The measurement gave a highly positive result. Because of this observation it is clear why the different concentration measurements do not follow a clear relationship between concentration of mutant DNA available and used EV number. This effect could be caused by EVs that break during storage in the freezer, which creates free mutant DNA fragments.

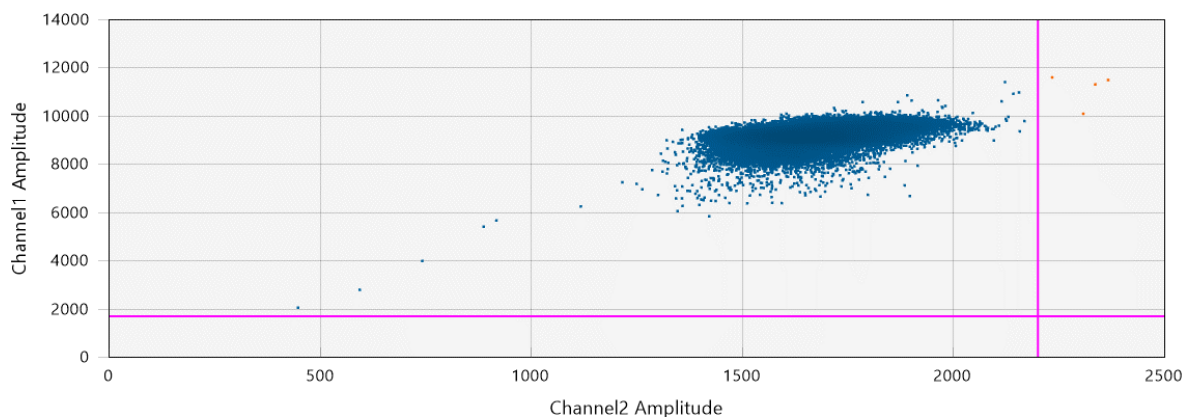


Figure 34. Free *EGFR* T790M mutation DNA bound to tip with igG isotype antibody

6 Discussion

In this project, the influence of a DNA stabilizing (Cell-free DNA) and RNA and EV stabilizing (RNA Complete) blood collection tube on DNA mutation detection in isolated PFP EVs was evaluated. Plasma derived EVs were isolated using two methods, qEV SEC and SmartSEC using samples from the two blood collection tubes on day of collection (day 0) and after 5 days of storage. Protein concentration analysis of these EV samples showed that the DNA BCT contained more proteins, but the concentration was independent of storage time for both BCTs. The total measured protein content varied strongly between different donors. Plasma protein concentration is highly dependent on demographical characteristics and pathological or physiological status of a blood donor (Spalding et al., 2018).

The number of EVs and the presence of EV- and platelet-EV membrane protein markers were analyzed in PFP EV samples that were directly processed, using high-sensitivity flow cytometry. The EV samples derived from the RNA BCT contained 29-67% CFDA-positive EVs, the DNA tube contained 9-18% of EVs in total particle number. The RNA BCT's EV population shows 80% positive CD41 particles, 79% CD81 particles and 37% CD9 particles. In the DNA BCT the EV population 23% of the EVs carries CD41, 20% CD81 and 18% CD9. The RNA BCT seems to be the most EV stabilizing BCT. It also seems that the PFP samples still do contain a large amount of platelet EVs (CD41). To remove more platelet EVs in the future an extra filtration step of the plasma on a 0,2 micron filter should be implemented after the centrifugation steps according to Stevanato et al. (1990).

A flow cytometry measurement on the blood samples collected and processed after 5 days still needs to be executed for EV quantities and available EV markers in the sample. This could give a good view on which tube is the best for hospital collections. But this still needs to be done on a larger scale in order to make real decisions.

A higher total protein amount does not directly indicate more EVs present in the tube. This higher protein amount can also derive from non-EV associated proteins. Using Western blot, we further assessed the presence of EV-specific and non-EV protein markers in the EV isolates. Western blot analysis revealed more cross-reaction of the CD9 antibody to other proteins present in the samples, across all the DNA BCT SEC fraction lanes. This could be attributed to the higher protein concentrations in these samples. Because the CD9 only appeared prominent in the DNA BCT after 5 days in this specific sample, it seems that when the plasma-EVs are not directly separated, this tube is less efficient in stabilizing the EVs. Also the detected CD9 may partially originate from platelet EVs, as Kim et al. (2022) have noted that CD9-positive EVs can be a blood platelet produced artifact. This confirms that the DNA BCT could be less efficient than the RNA BCT in stabilizing the collected blood sample for EV research, depending on the downstream analysis.

The western blot analysis on EV samples directly isolated on the day of blood collection did not reveal prominent differences between the different BCTs. The EV-marker CD9 was found in samples derived from both the DNA BCT and the RNA BCT and was a little bit more prominent in the RNA tube, non-EV markers calnexin and CD41 were not detected and lipid-protein complex marker was detected in both BCT samples.

Capture of EVs containing the EGFR T790M mutation on BLI tips was optimized and tested. This was done to perform immunocapture of plasma derived EV subpopulations and to check if they are present in sufficient amount for downstream analysis of their DNA content.

The optimization of the BLI-EV measurement was done by testing two antibodies. Concentration dependency was observed and confirmed by a linear correlation at 3000 seconds during the EV binding step. There is a clear correlation between larger negative signal and higher EV concentration. This was also confirmed with counterstaining using immune-conjugated gold nanoparticles. The tip functionalization with the antibody against CD81 was more successful: this antibody binds more on the SA tip, and it gives a 0.268 nm higher signal than the CD9 binding. Thus, CD81 can bind more EVs than CD9.

ddPCR measurements for DNA mutation detection in captured EVs still need to be optimized, since in these measurements no clear correlation could be found. A possible reason, for this is the presence of free DNA strands in the EV sample that can bind on the tips and be detected on ddPCR. EV stock samples were used on different days, which means that the EV integrity between measurements varies and can influence the presence of free DNA. After capture all EVs were lysed and free DNA can accidentally also be recovered from the tip during this step. After this lysis the ddPCR was performed.

Cell-free DNA was observed to have an influence on quantification of the *EGFR* T790M mutation. Therefore, to make sure that the measured mutated copy number only comes from the captured EVs, a DNase treatment could be implemented before EV lysis. This should remove the free DNA while leaving the EV-DNA unharmed, which is protected by the EV itself. This could make specific EV content evaluation possible.

CONCLUSION

The capture of tumor derived EVs and subsequent analysis of their mutational status can potentially lead to improved, more early detection of gene mutations in NSCLC patients. Two types of blood collection tubes were compared for their influence on the stability of plasma derived EV.

According to these findings it is possible to conclude that the cell-free DNA BCT stabilizes less EVs and thus degrades more EVs which causes a higher total protein concentration. While it seems that the RNA Complete BCT stabilizes more EVs according to flow cytometry results and the western blot at day 1 of one volunteer. This indicates that the RNA Complete BCTs are better for the follow up of the mutation status. Further research is needed to evaluate a larger number of blood samples and variations between different plasma samples.

In addition, it was evaluated whether bio-layer interferometry could be used to capture EVs and monitor the mutational status of these captured EVs using digital PCR. The used anti-CD81 antibodies captured the most EVs, this may be tested further in a complex medium like a plasma sample. The evaluation of mutational content in EVs with ddPCR needs to be tested with a DNase treatment of the EVs before lysis to remove free DNA strands. Our data confirm that the *EGFR* T790M DNA mutation is stably encapsulated and in high enough quantities for detection in the NCI-H1975 cell derived EVs. A promising next step would be capturing subpopulations of EVs with the help of disease-related markers and analyzing if an enrichment of mutation is visible within patient samples.

REFERENCE LIST

- Abels, E. R., & Breakefield, X. O. (2016). Introduction to Extracellular Vesicles: Biogenesis, RNA Cargo Selection, Content, Release, and Uptake. *Cell Mol Neurobiol*, 36(3), 301-312. <https://doi.org/10.1007/s10571-016-0366-z>
- AlQahtani, S. H., AlOgail, A. M., AlMosa, K. N., Alenazi, S. H., AlHasan, M. K., AlObaidan, R. H. et al. (2021). Frequency of Epidermal Growth Factor Receptor and T790M Mutations Among Patients With Non-Small Cell Lung Carcinoma: A Hospital-Based Study in the King Khalid University Hospital (KKUH) Since 2009-2017. *Cureus*, 13(11), e19816. <https://doi.org/10.7759/cureus.19816>
- Belgische Federale Overheidsdiensten (2021). *Daling van het aandeel hart- en vaatziekten als belangrijkste doodsoorzaak in 2018*. Statbel. Retrieved 14 March from <https://statbel.fgov.be/nl/themas/bevolking/sterfte-en-levensverwachting/doodsoorzaken#news>
- Bio-Rad. (2022). *Droplet Digital PCR Application Guide*. Bio-Rad Laboratories, Inc. Retrieved 17 February from https://www.bio-rad.com/webroot/web/pdf/lsr/literature/Bulletin_6407.pdf
- Biotechnologie, P. (2022). *Instructions Micro BCA Protein Assay Kit*. Thermo Fisher. Retrieved 1 May from https://www.thermofisher.com/document-connect/document-connect.html?url=https%3A%2F%2Fassets.thermofisher.com%2FTFS-Assets%2FMSG%2Fmanuals%2FMAN0011237_Micro_BCA_Protein_Asy_UG.pdf
- Bray, F., Ferlay, J., Soerjomataram, I., Siegel, R. L., Torre, L. A., & Jemal, A. (2018). Global cancer statistics 2018: GLOBOCAN estimates of incidence and mortality worldwide for 36 cancers in 185 countries. *CA Cancer J Clin*, 68(6), 394-424. <https://doi.org/10.3322/caac.21492>
- Chin, A. R., & Wang, S. E. (2016). Cancer-derived extracellular vesicles: the 'soil conditioner' in breast cancer metastasis? *Cancer Metastasis Rev*, 35(4), 669-676. <https://doi.org/10.1007/s10555-016-9639-8>
- Das, B. R., Bhaumik, S., Ahmad, F., Mandsaurwala, A., & Satam, H. (2015). Molecular spectrum of somatic EGFR and KRAS gene mutations in non small cell lung carcinoma: determination of frequency, distribution pattern and identification of novel variations in Indian patients. *Pathol Oncol Res*, 21(3), 675-687. <https://doi.org/10.1007/s12253-014-9874-7>
- Doyle, L. M., & Wang, M. Z. (2019). Overview of Extracellular Vesicles, Their Origin, Composition, Purpose, and Methods for Exosome Isolation and Analysis. *Cells*, 8(7), 727. <https://doi.org/10.3390/cells8070727>
- El Andaloussi, S., Mager, I., Breakefield, X. O., & Wood, M. J. (2013). Extracellular vesicles: biology and emerging therapeutic opportunities. *Nat Rev Drug Discov*, 12(5), 347-357. <https://doi.org/10.1038/nrd3978>
- Holcar, M., Kanduser, M., & Lenassi, M. (2021). Blood Nanoparticles - Influence on Extracellular Vesicle Isolation and Characterization [Review]. *Front Pharmacol*, 12, 773844. <https://doi.org/10.3389/fphar.2021.773844>
- Hur, J. Y., Kim, H. J., Lee, J. S., Choi, C. M., Lee, J. C., Jung, M. K. et al. (2018). Extracellular vesicle-derived DNA for performing EGFR genotyping of NSCLC patients. *Mol Cancer*, 17(1), 15. <https://doi.org/10.1186/s12943-018-0772-6>
- Interactions, C. f. M. (2022). *Biolayer Interferometry (BLI)*. Harvard Medical School. Retrieved 15 February from <https://cmi.hms.harvard.edu/biolayer-interferometry>
- IZON sciences (2022). *qEVoriginal user manual*. IZON Science LTD. Retrieved 26 April from https://www.schaefer-tec.it/sites/default/files/qEVoriginal_Technical_Note.pdf
- Jacobs, A. (2021). Standard Operating Procedure Kinetic assay on octet K2. In. VITO.
- Kim, H. J., Rames, M. J., Tassi Yunga, S., Armstrong, R., Morita, M., Ngo, A. T. P. et al. (2022). Irreversible alteration of extracellular vesicle and cell-free messenger RNA profiles in human plasma associated with blood processing and storage. *Sci Rep*, 12(1), 2099. <https://doi.org/10.1038/s41598-022-06088-9>

- Lacroix, R., Judicone, C., Mooberry, M., Boucekine, M., Key, N. S., Dignat-George, F. et al. (2013). Standardization of pre-analytical variables in plasma microparticle determination: results of the International Society on Thrombosis and Haemostasis SSC Collaborative workshop. *J Thromb Haemost*, 11(6), 1190-1193. <https://doi.org/10.1111/jth.12207>
- Lai, W. Y., Chen, C. Y., Yang, S. C., Wu, J. Y., Chang, C. J., Yang, P. C. et al. (2014). Overcoming EGFR T790M-based Tyrosine Kinase Inhibitor Resistance with an Allele-specific DNAzyme. *Mol Ther Nucleic Acids*, 3, e150. <https://doi.org/10.1038/mtna.2014.3>
- Lotvall, J., Hill, A. F., Hochberg, F., Buzas, E. I., Di Vizio, D., Gardiner, C. et al. (2014). Minimal experimental requirements for definition of extracellular vesicles and their functions: a position statement from the International Society for Extracellular Vesicles. *J Extracell Vesicles*, 3(Issue 1), 26913. <https://doi.org/10.3402/jev.v3.26913>
- Lu, X., Yu, L., Zhang, Z., Ren, X., Smail, J. B., & Ding, K. (2018). Targeting EGFR(L858R/T790M) and EGFR(L858R/T790M/C797S) resistance mutations in NSCLC: Current developments in medicinal chemistry. *Med Res Rev*, 38(5), 1550-1581. <https://doi.org/10.1002/med.21488>
- Neven, K. Y., Nawrot, T. S., & Bollati, V. (2017). Extracellular Vesicles: How the External and Internal Environment Can Shape Cell-To-Cell Communication. *Curr Environ Health Rep*, 4(1), 30-37. <https://doi.org/10.1007/s40572-017-0130-7>
- Nicholson, R. I., Gee, J. M., & Harper, M. E. (2001). EGFR and cancer prognosis. *Eur J Cancer*, 37 Suppl 4, S9-15. [https://doi.org/10.1016/s0959-8049\(01\)00231-3](https://doi.org/10.1016/s0959-8049(01)00231-3)
- Palviainen, M., Saraswat, M., Varga, Z., Kitka, D., Neuvonen, M., Puhka, M. et al. (2020). Extracellular vesicles from human plasma and serum are carriers of extravesicular cargo-Implications for biomarker discovery. *PLoS One*, 15(8), e0236439. <https://doi.org/10.1371/journal.pone.0236439>
- Punnoose, E. A., Atwal, S., Liu, W., Raja, R., Fine, B. M., Hughes, B. G. et al. (2012). Evaluation of circulating tumor cells and circulating tumor DNA in non-small cell lung cancer: association with clinical endpoints in a phase II clinical trial of pertuzumab and erlotinib. *Clin Cancer Res*, 18(8), 2391-2401. <https://doi.org/10.1158/1078-0432.CCR-11-3148>
- Ricordel, C., Friboulet, L., Facchinetti, F., & Soria, J. C. (2018). Molecular mechanisms of acquired resistance to third-generation EGFR-TKIs in EGFR T790M-mutant lung cancer. *Ann Oncol*, 29(suppl_1), i28-i37. <https://doi.org/10.1093/annonc/mdx705>
- Schubert, A., & Boutros, M. (2021). Extracellular vesicles and oncogenic signaling. *Mol Oncol*, 15(1), 3-26. <https://doi.org/10.1002/1878-0261.12855>
- Smart SEC System (2022). *SmartSEC® HT EV Isolation System for Serum & Plasma user manual*. System Biosciences, LLC. Retrieved 28 April from <https://www.systembio.com/products/exosome-research/exosome-isolation/smartsec/smartsec-ht-ev-isolation-system-for-serum-plasma>
- Song, H. N., Jung, K. S., Yoo, K. H., Cho, J., Lee, J. Y., Lim, S. H. et al. (2016). Acquired C797S Mutation upon Treatment with a T790M-Specific Third-Generation EGFR Inhibitor (HM61713) in Non-Small Cell Lung Cancer. *J Thorac Oncol*, 11(4), e45-47. <https://doi.org/10.1016/j.jtho.2015.12.093>
- Spalding, K., Bonnier, F., Bruno, C., Blasco, H., Board, R., Benz-de Bretagne, I. et al. (2018). Enabling quantification of protein concentration in human serum biopsies using attenuated total reflectance - Fourier transform infrared (ATR-FTIR) spectroscopy. *Vibrational Spectroscopy*, 99, 50-58. <https://doi.org/10.1016/j.vibspec.2018.08.019>
- Stevanato, F., Paolini, R., Fabris, F., Casonato, A., & Cella, G. (1990). Effect of cellulose acetate 0.2 micron filter on platelet specific proteins plasma levels. *Folia Haematol Int Mag Klin Morphol Blutforsch*, 117(3), 377-381. <https://www.ncbi.nlm.nih.gov/pubmed/1703106>
- Thakur, B. K., Zhang, H., Becker, A., Matei, I., Huang, Y., Costa-Silva, B. et al. (2014). Double-stranded DNA in exosomes: a novel biomarker in cancer detection. *Cell Res*, 24(6), 766-769. <https://doi.org/10.1038/cr.2014.44>

- Thery, C., Witwer, K. W., Aikawa, E., Alcaraz, M. J., Anderson, J. D., Andriantsitohaina, R. et al. (2018). Minimal information for studies of extracellular vesicles 2018 (MISEV2018): a position statement of the International Society for Extracellular Vesicles and update of the MISEV2014 guidelines. *J Extracell Vesicles*, 7(1), 1535750. <https://doi.org/10.1080/20013078.2018.1535750>
- Tian, Y., Gong, M., Hu, Y., Liu, H., Zhang, W., Zhang, M. et al. (2020). Quality and efficiency assessment of six extracellular vesicle isolation methods by nano-flow cytometry. *J Extracell Vesicles*, 9(1), 1697028. <https://doi.org/10.1080/20013078.2019.1697028>
- Tong, Y., Shen, S., Jiang, H., & Chen, Z. (2017). Application of Digital PCR in Detecting Human Diseases Associated Gene Mutation. *Cell Physiol Biochem*, 43(4), 1718-1730. <https://doi.org/10.1159/000484035>
- Travis, W. D., Brambilla, E., Noguchi, M., Nicholson, A. G., Geisinger, K., Yatabe, Y. et al. (2013). Diagnosis of lung cancer in small biopsies and cytology: implications of the 2011 International Association for the Study of Lung Cancer/American Thoracic Society/European Respiratory Society classification. *Arch Pathol Lab Med*, 137(5), 668-684. <https://doi.org/10.5858/arpa.2012-0263-RA>
- Tsatsaronis, J. A., Franch-Arroyo, S., Resch, U., & Charpentier, E. (2018). Extracellular Vesicle RNA: A Universal Mediator of Microbial Communication? *Trends Microbiol*, 26(5), 401-410. <https://doi.org/10.1016/j.tim.2018.02.009>
- van Niel, G., D'Angelo, G., & Raposo, G. (2018). Shedding light on the cell biology of extracellular vesicles. *Nat Rev Mol Cell Biol*, 19(4), 213-228. <https://doi.org/10.1038/nrm.2017.125>
- Wallner, J., Sissolak, B., Sommeregger, W., Lingg, N., Striedner, G., & Vorauer-Uhl, K. (2019). Lectin bio-layer interferometry for assessing product quality of Fc- glycosylated immunoglobulin G. *Biotechnol Prog*, 35(5), e2864. <https://doi.org/10.1002/btpr.2864>
- Walter, A. O., Sjin, R. T., Haringsma, H. J., Ohashi, K., Sun, J., Lee, K. et al. (2013). Discovery of a mutant-selective covalent inhibitor of EGFR that overcomes T790M-mediated resistance in NSCLC. *Cancer Discov*, 3(12), 1404-1415. <https://doi.org/10.1158/2159-8290.CD-13-0314>
- Wan, Y., Liu, B., Lei, H., Zhang, B., Wang, Y., Huang, H. et al. (2018). Nanoscale extracellular vesicle-derived DNA is superior to circulating cell-free DNA for mutation detection in early-stage non-small-cell lung cancer. *Ann Oncol*, 29(12), 2379-2383. <https://doi.org/10.1093/annonc/mdy458>
- Wang, X., Liu, H., Shen, Y., Li, W., Chen, Y., & Wang, H. (2018). Low-dose computed tomography (LDCT) versus other cancer screenings in early diagnosis of lung cancer: A meta-analysis. *Medicine (Baltimore)*, 97(27), e11233. <https://doi.org/10.1097/MD.00000000000011233>
- Yanez-Mo, M., Siljander, P. R., Andreu, Z., Zavec, A. B., Borrás, F. E., Buzas, E. I. et al. (2015). Biological properties of extracellular vesicles and their physiological functions. *J Extracell Vesicles*, 4(1), 27066. <https://doi.org/10.3402/jev.v4.27066>
- Yuan, G., Xie, H., Wei, T., Zhu, D., Zhang, C., & Yang, Y. (2021). Diagnostic potential of extracellular vesicle-associated microRNA-10b and tumor markers for lung adenocarcinoma. *Oncol Lett*, 22(2), 614. <https://doi.org/10.3892/ol.2021.12875>
- Zaborowski, M. P., Balaj, L., Breakefield, X. O., & Lai, C. P. (2015). Extracellular Vesicles: Composition, Biological Relevance, and Methods of Study. *BioScience*, 65(8), 783-797. <https://doi.org/10.1093/biosci/biv084>
- Zhang, Z., Stiegler, A. L., Boggon, T. J., Kobayashi, S., & Halmos, B. (2010). EGFR-mutated lung cancer: a paradigm of molecular oncology. *Oncotarget*, 1(7), 497-514. <https://doi.org/10.18632/oncotarget.186>

ATTACHMENTS

Attachment 1. MISEV 2018 guidelines of EV proteins (Thery et al., 2018)

Table 3. Protein content-based EV characterization. At least one protein of categories 1a or 1b, 2a (optionally 2b), 3a or 3b must be analysed to demonstrate the EV nature and the degree of purity of an EV preparation. Analysis of proteins of category 4 is required when claiming specific analysis of small EVs, and of category 5 to document functional activities. Examples of proteins commonly found in mammalian cell-derived EVs are provided, but other proteins that fall into the provided categories can be used, particularly for analysis of EVs from prokaryotic (bacteria) or non-mammalian eukaryotic sources (including parasites and plants). *XX** = human gene names. *XX*** or *XX**** used for families of multiple proteins, for example for integrins: *ITGA** indicates any integrin alpha chain.

Category	1- Transmembrane or GPI-anchored proteins associated to plasma membrane and/or endosomes	2- Cytosolic proteins recovered in EVs	3- Major components of non-EV co-isolated structures	4- Transmembrane, lipid-bound and soluble proteins associated to other intracellular compartments than PM/endosomes	5- Secreted proteins recovered with EVs
Use for	All EVs	All EVs	All EVs as purity control	Subtypes of EVs (e.g. large oncosomes, large EVs) and/or pathologic/atypical state	Functional component of EVs: need to determine the mode of association with EVs
1a:	non-tissue specific. Tetraspanins (CD63, CD81, CD82); other multi-pass membrane proteins (CD47; heterotrimeric G proteins <i>GNA**</i>)	2a: with lipid or membrane protein-binding ability. ESCRT-III/III (<i>TSG101</i> , <i>CHMP**</i>) and accessory proteins: <i>ALIX</i> (<i>PDZCD6IP</i>), <i>VP54A/B</i> ; <i>ARRDC1</i> ; <i>Flotillin-1</i> and <i>2</i> (<i>FLOT1/2</i>); <i>caveolins</i> (<i>CAV**</i>); <i>EHD*</i> ; <i>RHOA</i> ; <i>amexins</i> (<i>AMXA**</i>); <i>Heat shock proteins</i> <i>HSC70</i> (<i>HSPA8</i>), and <i>HSP84</i> (<i>HSP90AB1</i>) note that both are abundant also in exosomes; <i>ARF6</i> ; <i>synenin</i> (<i>SDCBP</i>); <i>microtubule-associated Tau</i> (<i>MAPT</i> , neurons)	3a: lipoproteins (produced by liver, abundant in plasma, serum). Apolipoproteins <i>A1/2</i> and <i>B</i> <i>APOA1/2</i> , <i>APOB</i> ; <i>APOB100</i> ; albumin (<i>ALB</i>)	4a: nucleus. Histones (<i>HIST1H**</i>); Lamin <i>A/C</i> (<i>LMNA</i>)	5a: Cytokines and growth factors. e.g. <i>TGFB1/2</i> ; <i>FGF</i> , <i>VEGFA</i> , <i>FGF1/2</i> , <i>PDGF*</i> , <i>EGF</i> , interleukins (<i>IL*</i>),...
1b:	cell/tissue specific. Some TSPANs: <i>TSPAN8</i> (epithelial cell), <i>CD37</i> and <i>CD53</i> (leukocytes), <i>CD9</i> (absent from NK, B and some MSC); <i>PECAM1</i> (endothelial cells); <i>ERBB2</i> (breast cancer); <i>EFCAM1</i> (epithelial); <i>CD90</i> (<i>THY1</i>) (MSCs); <i>CD45</i> (<i>PTPRC</i>) (immune cells), <i>CD41</i> (<i>ITGA2B</i>) or <i>CD42a</i> (<i>GP9</i>) (platelets); <i>Glycophorin A</i> (<i>GYPA</i>) (<i>RBG</i>); <i>CD14</i> (monocytes), <i>MHC class II</i> (<i>HLA-DR</i>)/ <i>DP/DQ</i> , <i>H2-A*</i>); <i>CD3*</i> (T cells); <i>Acetylcholinesterase/AChE-S</i> (neurons), <i>AChE-E</i> (erythrocytes); <i>amyloid beta A4/APP</i> (neurons); <i>multidrug resistance-associated protein</i> (<i>ABCC1</i>)	2b: promiscuous incorporation in EVs (and possibly exosomes). Heat shock protein <i>HSP70</i> (<i>HSPA1A</i>), cytoskeleton: <i>actin</i> (<i>ACT*</i>), <i>tubulin</i> (<i>TUB*</i>); enzymes (<i>GAPDH</i>)	3b: protein and protein/nucleic acid aggregates. <i>Tamm-Horsfall protein</i> (<i>Uromodulin/UMOD</i>) (urine); ribosomal proteins	4b: mitochondria <i>#MMT</i> , <i>cytochrome C</i> (<i>CYC1</i>); <i>TOMM20</i>	5b: adhesion and extracellular matrix proteins. <i>Fibronectin</i> (<i>FN1</i>), <i>Collagen</i> (<i>COL**</i>), <i>MFG8</i> ; <i>galactin3-binding protein</i> (<i>LGALS3BP</i>), <i>CD5L</i> ; <i>fetuin-A</i> (<i>AHSG</i>)
				4c: secretory pathway (endoplasmic reticulum, Golgi apparatus) <i>calnexin</i> (<i>CANX</i>); <i>Grp94</i> (<i>HSP90B1</i>); <i>BIP</i> (<i>HSPA5</i>), <i>GMI130</i> (<i>GOLGA2</i>)	
				4d: others (autophagosomes, cytoskeleton...), <i>ATG9A</i> , <i>Actinin1/4</i> (<i>ACTN1/4</i>), <i>cytokeratin 18</i> (<i>KRT18</i>)	

Attachment 2. Measured absorbances and calculated concentrations plasma donors A, B and C

A	Absorbance	Concentration (ng/μl)
DNA qEV 1	0,18	17,66
DNA qEV 2	0,28	46,46
DNA qEV 3	0,50	111,40
DNA qEV 4	0,86	216,91
DNA SMS 1	0,28	2283,14
DNA SMS 2	0,25	1925,34
RNA qEV 1	0,13	3,26
RNA qEV 2	0,22	28,24
RNA qEV 3	0,47	101,71
RNA qEV 4	0,76	188,40
RNA SMS 1	0,25	1952,34
RNA SMS 2	0,24	1756,56

B	Absorbance	Concentration (ng/μl)
DNA qEV 1	0,15	7,96
DNA qEV 2	0,24	35,88
DNA qEV 3	0,45	97,89
DNA qEV 4	0,75	184,87
DNA SMS 1	0,38	3714,35
DNA SMS 2	0,28	2343,90
RNA qEV 1	0,14	6,20
RNA qEV 2	0,23	33,53
RNA qEV 3	0,44	93,77
RNA qEV 4	0,79	197,80
RNA SMS 1	0,72	3343,04
RNA SMS 2	0,63	2235,88

C	Absorbance	Concentration (ng/μl)
DNA qEV1	0,355	87,20
DNA qEV2	0,492	143,92
DNA qEV3	1,030	366,85
DNA qEV4	2,094	807,12
RNA qEV1	0,161	7,09
RNA qEV2	0,285	58,43
RNA qEV3	0,610	192,77
RNA qEV4	1,276	468,48
5DNA qEV1	0,249	43,32
5DNA qEV2	0,557	170,82
5DNA qEV3	0,953	334,76
5DNA qEV4	2,002	769,04
5RNA qEV1	0,176	13,30
5RNA qEV2	0,322	73,54
5RNA qEV3	0,645	207,26
5RNA qEV4	1,424	529,75

Attachment 3. Flow cytometry results cell-free DNA BCT corrected for noise

							1/100			
		All	CFDA+	% CFD A	CD81- PECy7+	% CD81+	CD9- PECy7+	% CD9+	CD41- PECy7+	% CD41+
A (PBS + CFDA)										
	gem	49182	474							
B (PBS + CFDA+ CD81-PECy7)										
	gem	65785	704		501					
C (EV + CFDA)		96757	17243	17,82						
		87434	15933	18,22						
		90387	16181	17,90						
	gem	91526	16453	17,98						
	SD	4765	696	0,21						
D (EV + CFDA + CD81- PECy7)		73367	7381	10,06	1410	19,11				
		77019	7426	9,64	1474	19,85				
		75969	7821	10,29	1551	19,84				
	gem	75452	7542	10,00	1479	19,60				
	SD	1880	242	0,33	71	0,43				
E (EV + CFDA + CD9- PECy7)		189494	12541	6,62			3506	27,96		
		161003	23492	14,59			3221	13,71		
		156530	23097	14,76			3016	13,06		
	gem	169009	19710	11,99			3248	18,24		
	SD	17881	6212	4,65			246	8,42		
F (EV + CFDA + CD41- PECy7)		89963	8153	9,06					1894	23,24
		90783	8460	9,32					1888	22,32
		88744	8582	9,67					1972	22,98
	gem	89830	8398	9,35					1918	22,85
	SD	1026	221	0,31					47	0,47

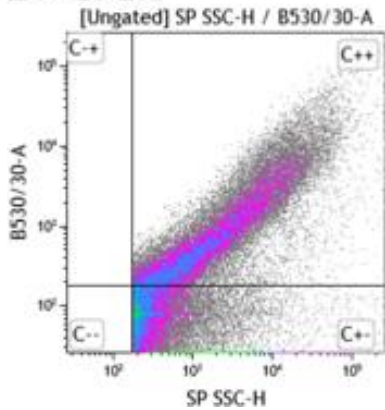
Attachment 4. Flow cytometry results RNA BCT corrected for noise

	1/200								
	All	CFDA+	% CFDA	CD81-PECy7+	% CD81+	CD9-PECy7+	% CD9+	CD41-PECy7+	% CD41+
A (PBS + CFDA)									
	gem	52033	546						
B (PBS + CFDA+ CD81-PECy7)									
	gem	59488	649		629				
C (EV + CFDA)		47999	18339	38,21					
		42361	17201	40,60					
		41040	17222	41,96					
	gem	43800	17587	40,26					
	SD	3696	651	1,90					
D (EV + CFDA + CD81-PECy7)		36299	9411	25,93	7302	77,59			
		27631	8514	30,81	6678	78,44			
		26589	8096	30,45	6595	81,46			
	gem	30173	8674	29,06	6859	79,16			
	SD	5331	672	2,72	386	2,03			
E (EV + CFDA + CD9-PECy7)		25550	7499	29,35			4990	66,54	
		29419	23492	79,85			5222	22,23	
		25224	23097	91,57			4789	20,74	
	gem	26731	18029	66,92			5001	36,50	
	SD	2334	9121	33,06			217	26,03	
F (EV + CFDA + CD41-PECy7)		20120	8454	42,02				6421	75,95
		24162	7190	29,76				5915	82,27
		11320	6482	57,26				5256	81,09
	gem	18534	7376	43,01				5864	79,77
	SD	6566	999	13,78				584	3,36

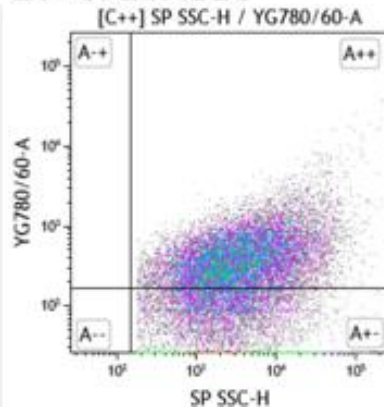
Attachment 5. Flow cytometry results H1975 SEC+UC EV stock corrected for noise + PE/Cy7[®] signal plots

		1/100						
		All	CFDA+	% CFDA	CD9-PECy7+	% CD9+	CD81-PECy7+	% CD81+
A (PBS + CFDA)								
	gem	34993,67	352					
B (PBS + CFDA+ CD81-PECy7)								
	gem	36694	377				373	
C (EV + CFDA)								
		43781,33	34572	78,96				
		45903,33	37413	81,50				
		44275,33	37202	84,02				
	gem	44653,33	36395	81,50				
	SD	1110	1583	2,53				
D (EV + CFDA + CD9-PECy7)								
		28816	21483	74,55	12440	57,91		
		28592	21348	74,66	12389	58,03		
		26353	20646	78,34	11965	57,95		
	gem	27920,67	21159	75,85	12265	57,96		
	SD	1362	449	2,16	261	0,06		
E (EV + CFDA + CD81-PECy7)								
		40769	23767	58,30			9781	41,15
		38468	23492	61,07			9305	39,61
		36625	23097	63,06			9114	39,46
	gem	38621	23452	60,81			9400	40,07
	SD	2076	337	2,39			343	0,94

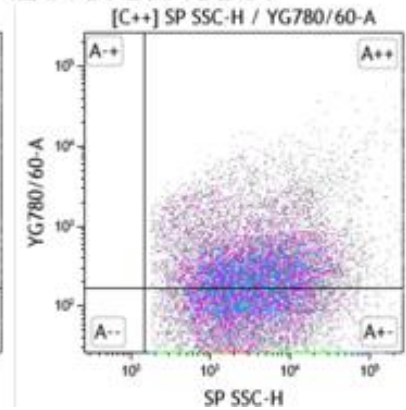
EV+CFDA




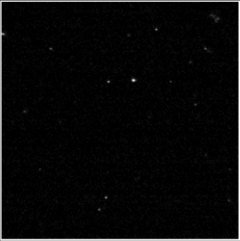
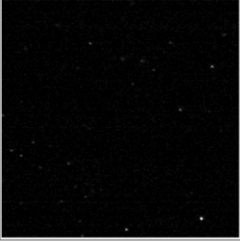
EV+CFDA+CD9





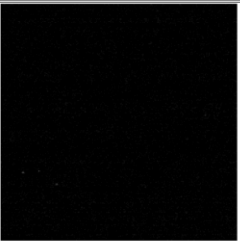
EV+CFDA+CD81



Attachment 6. NTA of EV SEC+UC stock CD9

<p>Sample Parameters Sample Name: 220511_EVnieuwestock_1-5000_fluo Comment: Sample Remarks0: Sample Remarks1: Sample Remarks2: Electrolyte: Temperature: 21,96 °C sensed pH 7,0 entered Conductivity: 293,44 µS/cm sensed</p> <p>Instrument Parameters Laser Wavelength: 488 nm Filter Wavelength: 500 nm</p> <p>Measurement Parameters Cell S/N: ZNTA</p> <p>Measurement Mode: Size Distribution 1 Cycle 11 Positions</p>	<p>Result (sizes in nm)</p> <table border="1"> <thead> <tr> <th>Number</th> <th>Concentration</th> <th>Volume</th> </tr> </thead> <tbody> <tr> <td>Median (X50)</td> <td>89,7</td> <td>206,7</td> </tr> <tr> <td>Span</td> <td>59,2</td> <td>93,5</td> </tr> </tbody> </table> <p>Concentration: 7,1E+7 Particles / mL Dilution Factor: 5000 Original Concentration: 3,5E+11 Particles / mL</p> <p>Quality Average Counted Particles per Frame: 182 Number of Traced Particles: 562</p> <p>Analysis Parameters Max Area: 1000, Min Area: 10, Min Brightness: 25</p>	Number	Concentration	Volume	Median (X50)	89,7	206,7	Span	59,2	93,5																																			
Number	Concentration	Volume																																											
Median (X50)	89,7	206,7																																											
Span	59,2	93,5																																											
<p>Peak Analysis (Concentration)</p> <table border="1"> <thead> <tr> <th>Diameter / nm</th> <th>Particles/mL</th> <th>FWHM / nm</th> <th>Percentage</th> </tr> </thead> <tbody> <tr> <td>74,7</td> <td>3,9E+6</td> <td>70,0</td> <td>76,0</td> </tr> <tr> <td>146,4</td> <td>1,4E+6</td> <td>23,7</td> <td>15,9</td> </tr> <tr> <td>203,7</td> <td>5,5E+5</td> <td>25,6</td> <td>8,1</td> </tr> </tbody> </table> <p>X Values (all sizes are given in nm)</p> <table border="1"> <thead> <tr> <th></th> <th>Number</th> <th>Concentration</th> <th>Volume</th> </tr> </thead> <tbody> <tr> <td>X10</td> <td>50,5</td> <td>50,5</td> <td>102,2</td> </tr> <tr> <td>X50</td> <td>89,7</td> <td>89,7</td> <td>206,7</td> </tr> <tr> <td>X90</td> <td>177,3</td> <td>177,3</td> <td>352,3</td> </tr> <tr> <td>Span</td> <td>1,4</td> <td>1,4</td> <td>1,2</td> </tr> <tr> <td>Mean</td> <td>108,2</td> <td>108,2</td> <td>225,9</td> </tr> <tr> <td>StdDev</td> <td>59,2</td> <td>59,1</td> <td>93,5</td> </tr> </tbody> </table> <p>Comment</p>	Diameter / nm	Particles/mL	FWHM / nm	Percentage	74,7	3,9E+6	70,0	76,0	146,4	1,4E+6	23,7	15,9	203,7	5,5E+5	25,6	8,1		Number	Concentration	Volume	X10	50,5	50,5	102,2	X50	89,7	89,7	206,7	X90	177,3	177,3	352,3	Span	1,4	1,4	1,2	Mean	108,2	108,2	225,9	StdDev	59,2	59,1	93,5	 <p>(Signature)</p>
Diameter / nm	Particles/mL	FWHM / nm	Percentage																																										
74,7	3,9E+6	70,0	76,0																																										
146,4	1,4E+6	23,7	15,9																																										
203,7	5,5E+5	25,6	8,1																																										
	Number	Concentration	Volume																																										
X10	50,5	50,5	102,2																																										
X50	89,7	89,7	206,7																																										
X90	177,3	177,3	352,3																																										
Span	1,4	1,4	1,2																																										
Mean	108,2	108,2	225,9																																										
StdDev	59,2	59,1	93,5																																										
<p>Sample Parameters Sample Name: 220511_EVnieuwestock_1-5000_fluo Comment: Sample Remarks0: Sample Remarks1: Sample Remarks2: Electrolyte: Temperature: 22,00 °C sensed pH 7,0 entered Conductivity: 312,16 µS/cm sensed</p> <p>Instrument Parameters Laser Wavelength: 488 nm Filter Wavelength: 500 nm</p> <p>Measurement Parameters Cell S/N: ZNTA</p> <p>Measurement Mode: Size Distribution 1 Cycle 11 Positions, 1 Removed for Analysis</p>	<p>Result (sizes in nm)</p> <table border="1"> <thead> <tr> <th>Number</th> <th>Concentration</th> <th>Volume</th> </tr> </thead> <tbody> <tr> <td>Median (X50)</td> <td>92,5</td> <td>205,3</td> </tr> <tr> <td>Span</td> <td>59,3</td> <td>104,5</td> </tr> </tbody> </table> <p>Concentration: 8,0E+7 Particles / mL Dilution Factor: 5000 Original Concentration: 4,0E+11 Particles / mL</p> <p>Quality Average Counted Particles per Frame: 207 Number of Traced Particles: 535</p> <p>Analysis Parameters Max Area: 1000, Min Area: 10, Min Brightness: 25</p>	Number	Concentration	Volume	Median (X50)	92,5	205,3	Span	59,3	104,5																																			
Number	Concentration	Volume																																											
Median (X50)	92,5	205,3																																											
Span	59,3	104,5																																											
<p>Peak Analysis (Concentration)</p> <table border="1"> <thead> <tr> <th>Diameter / nm</th> <th>Particles/mL</th> <th>FWHM / nm</th> <th>Percentage</th> </tr> </thead> <tbody> <tr> <td>74,7</td> <td>4,7E+6</td> <td>70,0</td> <td>76,0</td> </tr> <tr> <td>146,4</td> <td>1,7E+6</td> <td>23,7</td> <td>15,9</td> </tr> <tr> <td>203,7</td> <td>6,5E+5</td> <td>25,6</td> <td>8,1</td> </tr> </tbody> </table> <p>X Values (all sizes are given in nm)</p> <table border="1"> <thead> <tr> <th></th> <th>Number</th> <th>Concentration</th> <th>Volume</th> </tr> </thead> <tbody> <tr> <td>X10</td> <td>49,6</td> <td>49,6</td> <td>103,8</td> </tr> <tr> <td>X50</td> <td>92,5</td> <td>92,5</td> <td>205,3</td> </tr> <tr> <td>X90</td> <td>180,5</td> <td>180,5</td> <td>366,6</td> </tr> <tr> <td>Span</td> <td>1,4</td> <td>1,4</td> <td>1,3</td> </tr> <tr> <td>Mean</td> <td>109,3</td> <td>109,3</td> <td>229,4</td> </tr> <tr> <td>StdDev</td> <td>59,3</td> <td>59,3</td> <td>104,5</td> </tr> </tbody> </table> <p>Comment</p>	Diameter / nm	Particles/mL	FWHM / nm	Percentage	74,7	4,7E+6	70,0	76,0	146,4	1,7E+6	23,7	15,9	203,7	6,5E+5	25,6	8,1		Number	Concentration	Volume	X10	49,6	49,6	103,8	X50	92,5	92,5	205,3	X90	180,5	180,5	366,6	Span	1,4	1,4	1,3	Mean	109,3	109,3	229,4	StdDev	59,3	59,3	104,5	 <p>(Signature)</p>
Diameter / nm	Particles/mL	FWHM / nm	Percentage																																										
74,7	4,7E+6	70,0	76,0																																										
146,4	1,7E+6	23,7	15,9																																										
203,7	6,5E+5	25,6	8,1																																										
	Number	Concentration	Volume																																										
X10	49,6	49,6	103,8																																										
X50	92,5	92,5	205,3																																										
X90	180,5	180,5	366,6																																										
Span	1,4	1,4	1,3																																										
Mean	109,3	109,3	229,4																																										
StdDev	59,3	59,3	104,5																																										
<p>Sample Parameters Sample Name: 220511_EVnieuwestock_1-5000_fluo Comment: Sample Remarks0: Sample Remarks1: Sample Remarks2: Electrolyte: Temperature: 21,95 °C sensed pH 7,0 entered Conductivity: 300,36 µS/cm sensed</p> <p>Instrument Parameters Laser Wavelength: 488 nm Filter Wavelength: 500 nm</p> <p>Measurement Parameters Cell S/N: ZNTA</p> <p>Measurement Mode: Size Distribution 1 Cycle 11 Positions</p>	<p>Result (sizes in nm)</p> <table border="1"> <thead> <tr> <th>Number</th> <th>Concentration</th> <th>Volume</th> </tr> </thead> <tbody> <tr> <td>Median (X50)</td> <td>91,9</td> <td>199,9</td> </tr> <tr> <td>Span</td> <td>57,4</td> <td>96,2</td> </tr> </tbody> </table> <p>Concentration: 7,6E+7 Particles / mL Dilution Factor: 5000 Original Concentration: 3,8E+11 Particles / mL</p> <p>Quality Average Counted Particles per Frame: 195 Number of Traced Particles: 538</p> <p>Analysis Parameters Max Area: 1000, Min Area: 10, Min Brightness: 25</p>	Number	Concentration	Volume	Median (X50)	91,9	199,9	Span	57,4	96,2																																			
Number	Concentration	Volume																																											
Median (X50)	91,9	199,9																																											
Span	57,4	96,2																																											
<p>Peak Analysis (Concentration)</p> <table border="1"> <thead> <tr> <th>Diameter / nm</th> <th>Particles/mL</th> <th>FWHM / nm</th> <th>Percentage</th> </tr> </thead> <tbody> <tr> <td>74,7</td> <td>4,4E+6</td> <td>70,0</td> <td>76,0</td> </tr> <tr> <td>146,4</td> <td>1,6E+6</td> <td>23,7</td> <td>15,9</td> </tr> <tr> <td>203,7</td> <td>6,1E+5</td> <td>25,6</td> <td>8,1</td> </tr> </tbody> </table> <p>X Values (all sizes are given in nm)</p> <table border="1"> <thead> <tr> <th></th> <th>Number</th> <th>Concentration</th> <th>Volume</th> </tr> </thead> <tbody> <tr> <td>X10</td> <td>49,6</td> <td>49,6</td> <td>101,7</td> </tr> <tr> <td>X50</td> <td>91,9</td> <td>91,9</td> <td>199,9</td> </tr> <tr> <td>X90</td> <td>175,6</td> <td>175,6</td> <td>357,9</td> </tr> <tr> <td>Span</td> <td>1,4</td> <td>1,4</td> <td>1,3</td> </tr> <tr> <td>Mean</td> <td>107,7</td> <td>107,7</td> <td>220,4</td> </tr> <tr> <td>StdDev</td> <td>57,4</td> <td>57,4</td> <td>96,2</td> </tr> </tbody> </table> <p>Comment</p>	Diameter / nm	Particles/mL	FWHM / nm	Percentage	74,7	4,4E+6	70,0	76,0	146,4	1,6E+6	23,7	15,9	203,7	6,1E+5	25,6	8,1		Number	Concentration	Volume	X10	49,6	49,6	101,7	X50	91,9	91,9	199,9	X90	175,6	175,6	357,9	Span	1,4	1,4	1,3	Mean	107,7	107,7	220,4	StdDev	57,4	57,4	96,2	 <p>(Signature)</p>
Diameter / nm	Particles/mL	FWHM / nm	Percentage																																										
74,7	4,4E+6	70,0	76,0																																										
146,4	1,6E+6	23,7	15,9																																										
203,7	6,1E+5	25,6	8,1																																										
	Number	Concentration	Volume																																										
X10	49,6	49,6	101,7																																										
X50	91,9	91,9	199,9																																										
X90	175,6	175,6	357,9																																										
Span	1,4	1,4	1,3																																										
Mean	107,7	107,7	220,4																																										
StdDev	57,4	57,4	96,2																																										

Attachment 7. NTA of New EV SEC+UC stock CD81

<p>Sample Parameters Sample Name: 220309_EVH1975_1-6000_fluo Comment: Sample Remarks0: Sample Remarks1: Sample Remarks2: Electrolyte: Temperature: 21,98 °C sensed pH 7,0 entered Conductivity: 201,21 µS/cm sensed</p> <p>Measurement Parameters Cell S/N: ZNTA</p> <p>Measurement Mode: Size Distribution 1 Cycle 11 Positions</p>	<p>Result (sizes in nm)</p> <table border="1"> <thead> <tr> <th></th> <th>Number</th> <th>Concentration</th> <th>Volume</th> </tr> </thead> <tbody> <tr> <td>Median (X50)</td> <td>123,3</td> <td>123,3</td> <td>349,0</td> </tr> <tr> <td>Span</td> <td>86,6</td> <td>86,6</td> <td>376,2</td> </tr> </tbody> </table> <p>Concentration: 3,9E+7 Particles / mL Dilution Factor: 1 Original Concentration: 3,9E+7 Particles / mL</p> <p>Quality Average Counted Particles per Frame: 100 Number of Traced Particles: 639</p> <p>Analysis Parameters Max Area: 1000, Min Area: 10, Min Brightness: 25</p>		Number	Concentration	Volume	Median (X50)	123,3	123,3	349,0	Span	86,6	86,6	376,2																								
	Number	Concentration	Volume																																		
Median (X50)	123,3	123,3	349,0																																		
Span	86,6	86,6	376,2																																		
<p>Peak Analysis (Concentration)</p> <table border="1"> <thead> <tr> <th>Diameter / nm</th> <th>Particles/mL</th> <th>FWHM / nm</th> <th>Percentage</th> </tr> </thead> <tbody> <tr> <td>115,0</td> <td>2,7E+6</td> <td>112,1</td> <td>100,0</td> </tr> </tbody> </table> <p>X Values (all sizes are given in nm)</p> <table border="1"> <thead> <tr> <th></th> <th>Number</th> <th>Concentration</th> <th>Volume</th> </tr> </thead> <tbody> <tr> <td>X10</td> <td>67,5</td> <td>67,5</td> <td>151,2</td> </tr> <tr> <td>X50</td> <td>123,3</td> <td>123,3</td> <td>349,0</td> </tr> <tr> <td>X90</td> <td>234,4</td> <td>234,4</td> <td>1121,0</td> </tr> <tr> <td>Span</td> <td>1,4</td> <td>1,4</td> <td>2,8</td> </tr> <tr> <td>Mean</td> <td>148,4</td> <td>148,4</td> <td>515,1</td> </tr> <tr> <td>StdDev</td> <td>86,6</td> <td>86,6</td> <td>376,2</td> </tr> </tbody> </table> <p>Comment</p>	Diameter / nm	Particles/mL	FWHM / nm	Percentage	115,0	2,7E+6	112,1	100,0		Number	Concentration	Volume	X10	67,5	67,5	151,2	X50	123,3	123,3	349,0	X90	234,4	234,4	1121,0	Span	1,4	1,4	2,8	Mean	148,4	148,4	515,1	StdDev	86,6	86,6	376,2	 <p>(Signature)</p>
Diameter / nm	Particles/mL	FWHM / nm	Percentage																																		
115,0	2,7E+6	112,1	100,0																																		
	Number	Concentration	Volume																																		
X10	67,5	67,5	151,2																																		
X50	123,3	123,3	349,0																																		
X90	234,4	234,4	1121,0																																		
Span	1,4	1,4	2,8																																		
Mean	148,4	148,4	515,1																																		
StdDev	86,6	86,6	376,2																																		
<p>Sample Parameters Sample Name: 220309_EVH1975_1-6000_fluo Comment: Sample Remarks0: Sample Remarks1: Sample Remarks2: Electrolyte: Temperature: 21,93 °C sensed pH 7,0 entered Conductivity: 215,02 µS/cm sensed</p> <p>Measurement Parameters Cell S/N: ZNTA</p> <p>Measurement Mode: Size Distribution 1 Cycle 11 Positions, 1 Removed for Analysis</p>	<p>Result (sizes in nm)</p> <table border="1"> <thead> <tr> <th></th> <th>Number</th> <th>Concentration</th> <th>Volume</th> </tr> </thead> <tbody> <tr> <td>Median (X50)</td> <td>125,9</td> <td>125,9</td> <td>300,5</td> </tr> <tr> <td>Span</td> <td>81,8</td> <td>81,8</td> <td>288,9</td> </tr> </tbody> </table> <p>Concentration: 3,4E+7 Particles / mL Dilution Factor: 1 Original Concentration: 3,4E+7 Particles / mL</p> <p>Quality Average Counted Particles per Frame: 86 Number of Traced Particles: 506</p> <p>Analysis Parameters Max Area: 1000, Min Area: 10, Min Brightness: 25</p>		Number	Concentration	Volume	Median (X50)	125,9	125,9	300,5	Span	81,8	81,8	288,9																								
	Number	Concentration	Volume																																		
Median (X50)	125,9	125,9	300,5																																		
Span	81,8	81,8	288,9																																		
<p>Peak Analysis (Concentration)</p> <table border="1"> <thead> <tr> <th>Diameter / nm</th> <th>Particles/mL</th> <th>FWHM / nm</th> <th>Percentage</th> </tr> </thead> <tbody> <tr> <td>115,0</td> <td>2,9E+6</td> <td>112,1</td> <td>100,0</td> </tr> </tbody> </table> <p>X Values (all sizes are given in nm)</p> <table border="1"> <thead> <tr> <th></th> <th>Number</th> <th>Concentration</th> <th>Volume</th> </tr> </thead> <tbody> <tr> <td>X10</td> <td>68,7</td> <td>68,7</td> <td>143,1</td> </tr> <tr> <td>X50</td> <td>125,9</td> <td>125,9</td> <td>300,5</td> </tr> <tr> <td>X90</td> <td>239,8</td> <td>239,8</td> <td>1115,9</td> </tr> <tr> <td>Span</td> <td>1,4</td> <td>1,4</td> <td>3,2</td> </tr> <tr> <td>Mean</td> <td>149,6</td> <td>149,6</td> <td>400,2</td> </tr> <tr> <td>StdDev</td> <td>81,8</td> <td>81,8</td> <td>288,9</td> </tr> </tbody> </table> <p>Comment</p>	Diameter / nm	Particles/mL	FWHM / nm	Percentage	115,0	2,9E+6	112,1	100,0		Number	Concentration	Volume	X10	68,7	68,7	143,1	X50	125,9	125,9	300,5	X90	239,8	239,8	1115,9	Span	1,4	1,4	3,2	Mean	149,6	149,6	400,2	StdDev	81,8	81,8	288,9	 <p>(Signature)</p>
Diameter / nm	Particles/mL	FWHM / nm	Percentage																																		
115,0	2,9E+6	112,1	100,0																																		
	Number	Concentration	Volume																																		
X10	68,7	68,7	143,1																																		
X50	125,9	125,9	300,5																																		
X90	239,8	239,8	1115,9																																		
Span	1,4	1,4	3,2																																		
Mean	149,6	149,6	400,2																																		
StdDev	81,8	81,8	288,9																																		
<p>Sample Parameters Sample Name: 220309_EVH1975_1-6000_fluo Comment: Sample Remarks0: Sample Remarks1: Sample Remarks2: Electrolyte: Temperature: 21,91 °C sensed pH 7,0 entered Conductivity: 207,31 µS/cm sensed</p> <p>Measurement Parameters Cell S/N: ZNTA</p> <p>Measurement Mode: Size Distribution 1 Cycle 11 Positions, 1 Removed for Analysis</p>	<p>Result (sizes in nm)</p> <table border="1"> <thead> <tr> <th></th> <th>Number</th> <th>Concentration</th> <th>Volume</th> </tr> </thead> <tbody> <tr> <td>Median (X50)</td> <td>126,4</td> <td>126,4</td> <td>325,2</td> </tr> <tr> <td>Span</td> <td>85,1</td> <td>85,1</td> <td>315,7</td> </tr> </tbody> </table> <p>Concentration: 3,7E+7 Particles / mL Dilution Factor: 1 Original Concentration: 3,7E+7 Particles / mL</p> <p>Quality Average Counted Particles per Frame: 94 Number of Traced Particles: 524</p> <p>Analysis Parameters Max Area: 1000, Min Area: 10, Min Brightness: 25</p>		Number	Concentration	Volume	Median (X50)	126,4	126,4	325,2	Span	85,1	85,1	315,7																								
	Number	Concentration	Volume																																		
Median (X50)	126,4	126,4	325,2																																		
Span	85,1	85,1	315,7																																		
<p>Peak Analysis (Concentration)</p> <table border="1"> <thead> <tr> <th>Diameter / nm</th> <th>Particles/mL</th> <th>FWHM / nm</th> <th>Percentage</th> </tr> </thead> <tbody> <tr> <td>115,0</td> <td>3,1E+6</td> <td>112,1</td> <td>100,0</td> </tr> </tbody> </table> <p>X Values (all sizes are given in nm)</p> <table border="1"> <thead> <tr> <th></th> <th>Number</th> <th>Concentration</th> <th>Volume</th> </tr> </thead> <tbody> <tr> <td>X10</td> <td>68,6</td> <td>68,6</td> <td>147,4</td> </tr> <tr> <td>X50</td> <td>126,4</td> <td>126,4</td> <td>325,2</td> </tr> <tr> <td>X90</td> <td>243,6</td> <td>243,6</td> <td>1118,1</td> </tr> <tr> <td>Span</td> <td>1,4</td> <td>1,4</td> <td>3,0</td> </tr> <tr> <td>Mean</td> <td>150,8</td> <td>150,8</td> <td>437,2</td> </tr> <tr> <td>StdDev</td> <td>85,1</td> <td>85,1</td> <td>315,7</td> </tr> </tbody> </table> <p>Comment</p>	Diameter / nm	Particles/mL	FWHM / nm	Percentage	115,0	3,1E+6	112,1	100,0		Number	Concentration	Volume	X10	68,6	68,6	147,4	X50	126,4	126,4	325,2	X90	243,6	243,6	1118,1	Span	1,4	1,4	3,0	Mean	150,8	150,8	437,2	StdDev	85,1	85,1	315,7	 <p>(Signature)</p>
Diameter / nm	Particles/mL	FWHM / nm	Percentage																																		
115,0	3,1E+6	112,1	100,0																																		
	Number	Concentration	Volume																																		
X10	68,6	68,6	147,4																																		
X50	126,4	126,4	325,2																																		
X90	243,6	243,6	1118,1																																		
Span	1,4	1,4	3,0																																		
Mean	150,8	150,8	437,2																																		
StdDev	85,1	85,1	315,7																																		

Attachment 8. Concentrations used in the CD9 BLI measurements (A) and concentrations used in the CD81 BLI measurements (B)

A

Concentration (particles/mL)	Volume of EV stock (μ L)	Volume of kinetics buffer (μ L)
1×10^{10}	12	438
1.5×10^{10}	17.9	432.1
2×10^{10}	23.9	426.1
3×10^{10}	35.8	414.2

B

concentration (particles/mL)	Volume of EV stock (μ L)	Volume of kinetics buffer (μ L)
1×10^{10}	20.9	429.1
1.5×10^{10}	31.3	418.7
2×10^{10}	41.7	408.3
3×10^{10}	62.6	387.4